A POSTERIORI ERROR ESTIMATES FOR TIME-DEPENDENT HAMILTON-JACOBI EQUATIONS

A DISSERTATION
SUBMITTED TO THE FACULTY OF THE GRADUATE SCHOOL
OF THE UNIVERSITY OF MINNESOTA
BY

IVAN GEORGIEV MEREV

IN PARTIAL FULFILLMENT OF THE REQUIREMENTS
FOR THE DEGREE OF

Doctor Of Philosophy

PROF. BERNARDO COCKBURN, Adviser

May, 2010

Acknowledgements

I am deeply indebted and very thankful to my PhD adviser Professor Bernardo Cockburn for his encouragement, support, guidance and enlightening conversations. It was an honor having Bernardo as an adviser and a friend. This dissertation would not have been possible without him.

I would also like to thank Professor Fernando Reitich, Professor Maria-Carme Calderer, Professor Marta Lewicka, Professor Yoichiro Mori and Professor Duane Nykamp for being on my examining committees and for their valuable advices. I am also very thankful to Professor Francisco Javier Sayas, my officemates Manuel Solano, Ke Shi, Wujun Zhang and my colleague and friend Jose Orozco for the encouragement, feedback and help during my six years at the University of Minnesota.

Many thanks to Iglika for her patience and unconditional support.

Finally, I owe everything to my parents Georgi and Kunka and my brother Apostol. Words are not enough to express how much they mean to me. They deserve great thanks for always being there for me.

Dedication

Dedicated to my father Georgi and my mother Kunka.

Abstract

We present a local a posteriori error estimate for general numerical methods for time-dependent Hamilton-Jacobi equations. Since Hamilton-Jacobi equations find applications in many areas there is an interest in constructing efficient algorithms that produce numerical approximations with a guaranteed precision set beforehand by the practitioner. To develop such algorithms, it is important to be able to estimate the quality of any given approximation in terms of computable quantities only, and this is what a posteriori error estimates provide. Given an arbitrary domain $\Omega \in \mathbb{R}^d$ and a time $T > 0$, the a posteriori error estimate gives an upper bound for the L^∞-norm of the difference between the viscosity solution u and any continuous function v in Ω at time T. The estimate holds for general Hamiltonians and any space dimensions d. The case $\Omega = \mathbb{R}^d$ reduces to the global a posteriori error estimate obtained by S. Albert, B. Cockburn, D. French, and T. Peterson in *A posteriori error estimates for general numerical methods for Hamilton-Jacobi equations. Part II: The time-dependent case*, Finite Volumes for Complex Applications, vol. III, June 2002, pp. 17–24. Numerical experiments investigating the sharpness of both the global and local a posteriori error estimates are provided. The results confirm that the a posteriori error estimates are very efficient and are thus an ideal tool for devising adaptive algorithms with rigorous error control for time-dependent Hamilton-Jacobi equations.

Table of Contents

List of Tables

List of Figures

Chapter 1

Introduction

Hamilton-Jacobi equations arise in many fields such as level set methods for analyzing and computing interface motions in computer vision, materials science, fluid mechanics, and image processing [25], optimization and continuous-time deterministic optimal control [5], [6], differential games [15], and, recently, finance [17], among others. The wide application of this type of equations requires the availability of robust and efficient numerical algorithms for solving them.

1.1 The problem and a review of the literature

The goal of this dissertation is to study a posteriori error estimates for time-dependent Hamilton-Jacobi equations. We develop a local a posteriori error estimate that gives an upper bound for the difference between the viscosity solution u of the following Cauchy problem for the model Hamilton-Jacobi equation;

$$u_t + H(x, \nabla u) = 0 \qquad \text{for } (x,t) \in \mathbb{R}^d \times (0,T), \tag{1.1}$$

$$u(x, t=0) = u_0(x) \qquad \text{for } x \in \mathbb{R}^d; \tag{1.2}$$

and any continuous function v. The estimate has the form

$$\| u(x,T) - v(x,T) \|_{L^\infty(\Omega)} \leq \Phi(v;T,\Omega), \tag{1.3}$$

where T is an arbitrary positive number, Ω is an arbitrary sub-domain of $\mathbb{R}^d$, and as expected, the functional Φ depends on the error on the domain of dependence at the initial time, the (shifted) residual of the function v on a domain that contains the union of all cones of dependence with vertices in Ω, and the smoothness of the function v. This result extends those obtained in [2] and [3]. Indeed, when $\Omega = \mathbb{R}^d$, our estimate becomes the global estimate obtained in [3], which was in turn obtained by extending to the time-dependent case the estimate for the steady-state case proposed in [2].

Several authors have obtained error estimates in the L^∞-norm for Hamilton-Jacobi equations, but the results obtained in [2] and [3], and, hence, the result in this dissertation, are different in many aspects. Crandall and Lions [13] obtained an a priori estimate for a monotone scheme defined in Cartesian grids for equations whose Hamiltonian functions depend on ∇u only. In our setting their result can be written in the form

$$\| u(x,T) - v(x,T) \|_{L^\infty(\Omega)} \leq C\sqrt{\Delta x}, \tag{1.4}$$

where Δx is the maximum mesh size and C is a constant that depends on the supremum of $|u_0|$, the numerical Hamiltonian of the scheme used, the terminal time T, and the Lipschitz constant of the initial condition u_0. Abgrall [1] introduced the intrinsic monotone schemes for unstructured meshes and proved that the same error estimate holds. Qian [24] proved that (1.4) holds for a modification of the classic Lax-Friedrichs scheme that allows for locally varying time and space grids. Falcone and Ferretti [16] obtained a priori error estimates for Hamilton-Jacobi-Bellman equations for schemes that were constructed by using the discrete

dynamic programming principle and were devised to converge very fast to the exact solution. They assume that the viscosity solution of the Hamilton-Jacobi-Bellman equation is very smooth, however, and their results apply only to convex Hamiltonians.

All these a priori error estimates are of little use in practical applications because they depend on the numerical method used to compute the approximate solution v, involve information that is *not known* about the exact solution, and cannot capture the features of the *particular* problem under consideration. In contrast, our a posteriori error estimate (1.3) and the a posteriori error estimates obtained in [2] and [3] hold regardless of how v is computed. They can thus be applied if v is obtained by means of a finite difference scheme like the ENO scheme developed by Osher and Shu [23], a finite element method like the discontinuous Galerkin (DG) method proposed by Hu and Shu [18], the Petrov-Galerkin method used by Barth and Sethian [4], or a finite volume method like the intrinsic monotone scheme of Abgrall [1]. These estimates are also independent of the smoothness of the exact solution, hold for general Hamiltonians and take into account the particularities of the specific problem. This makes them an ideal tool for devising adaptive algorithms with rigorous error control for Hamilton-Jacobi equations.

Error estimates using other than the L^∞-norm are rare. The reason is that the use of any other norm involves the resolution of the so-called adjoint equation. Lin and Tadmor [21] obtained an estimate in the L^1-norm and had to consider the resolution of an adjoint equation. They found its solution only in the case of a convex Hamiltonian, and, therefore, their error estimate holds only for convex Hamiltonians.

A posteriori error estimates allow for estimating the quality of any given numerical approximation in terms of computable quantities only. Sharp a posteriori error estimates are important in constructing adaptive schemes that produce numerical approximations with a guaranteed precision set beforehand by the practitioner. Given a tolerance $\tau > 0$, such an adaptive method has the following structure:

1. Construct an initial grid $\mathcal{D}_h$.
2. Compute an approximate solution u_h on the grid $\mathcal{D}_h$.
3. Compute the estimate of the error, $\Phi_h(u_h)$.
4. If $\Phi_h(u_h) \leq \tau$, **stop**.
5. Otherwise, compute a new grid $\mathcal{D}_h$ and go to 2.

Adaptive schemes of the form described above for time-dependent Hamilton-Jacobi equations have not been developed yet. The steady-state a posteriori error estimate obtained in [2] has been utilized in a few adaptive schemes. In [9] and [10] an adaptive method for one- and two-dimensional steady-state Hamilton-Jacobi equations using a monotone scheme was developed. An adaptive scheme for steady-state Hamilton-Jacobi equations using the discontinuous Galerkin (DG) method was proposed in [7]. Adaptive algorithms of different forms and purposes have been developed in [20] and [27]. In [20] different Godunov-type projection-evolution methods in different parts of the computational domain (these parts being determined adaptively as the mesh gets refined) were used in order to ensure the convergence of the approximate solution to the viscosity solution. In [27] an adaptive algorithm using a modification of the classic Lax-Friedrichs scheme

along with a suitable refinement of the mesh was developed to obtain an order of convergence of 2.

1.2 Applications of Hamilton-Jacobi equations

1.2.1 Level set formulation for propagating interfaces

An important area of application where time-dependent Hamilton-Jacobi equations arise concerns the tracking of the motion of evolving interfaces. We follow the development presented in [25]. Consider a closed N-dimensional hypersurface $\Gamma(t=0)$. The goal is to track the motion of the hypersurface $\Gamma(t)$ propagating along its normal direction with speed F, where F can be a function of a variety of arguments such as curvature, position, normal direction, etc. The idea is to embed this propagating interface as the zero level set of a higher dimensional function ϕ, i.e., we look for a function $\phi(\cdot,\cdot) : \mathbb{R}^N \times [0,\infty) \to \mathbb{R}$ such that the level set $\phi(\cdot,t) = 0$ gives $\Gamma(t)$.

Define $\phi(x, t=0)$ as

$$\phi(x, t=0) = \pm d,$$

where d is the distance from x to $\Gamma(t=0)$, and the plus (minus) sign is chosen if the point x is outside (inside) the initial hypersurface $\Gamma(t=0)$. Let $x(t)$ be the path of a point on the propagating front, i.e., $x(0)$ is a point on the initial front $\Gamma(t=0)$ and $x(t)$ is a point on $\Gamma(t)$. Since the motion is in the direction normal to the front, $x'(t) \cdot \vec{n} = F\left(x(t)\right)$, where the vector $x'(t)$ is normal to the front at $x(t)$. The fact that $\phi(\cdot,t)$ is zero on $\Gamma(t)$ means that

$$\phi\left(x(t),t\right) = 0.$$

Differentiating with respect to time we obtain

$$\phi_t + \nabla\phi(x(t), t) \cdot x'(t) = 0. \tag{1.5}$$

Since F is the speed in the outward normal direction, $x'(t) = F\,\vec{n}$, where the unit normal vector $\vec{n} = \nabla\phi/|\nabla\phi|$. Upon substituting in (1.5), we obtain

$$\phi_t + \nabla\phi(x(t), t) \cdot F\,\frac{\nabla\phi}{|\nabla\phi|} = 0,$$

i.e.,

$$\phi_t + F\,|\nabla\phi| = 0.$$

For certain forms of the speed function F, one obtains a standard time-dependent Hamilton-Jacobi equation with the initial condition $\phi(x, 0) = \pm d$. This formulation of the problem as opposed to the traditional Lagrangian approach of working with a parametrization of the boundary of the hypersurface $\Gamma(t)$ has an advantage in the cases when $\Gamma(t)$ changes topology as in the two-dimensional example shown in Figure 1.1.

Sethian [25] illustrates the above approach on a host of interesting examples from fluid mechanics, combustion, image processing, materials science, seismology, fabrication of microelectronic components, computer vision and a collection of other areas.

1.2.2 Continuous-time deterministic optimal control

Time-dependent Hamilton-Jacobi equations also arise in continuous-time deterministic optimal control. This section is a brief introduction to the subject. Below is a derivation of the so-called Hamilton-Jacobi-Bellman partial differential equation corresponding to a model continuous-time dynamic system. We follow the development presented in [5].

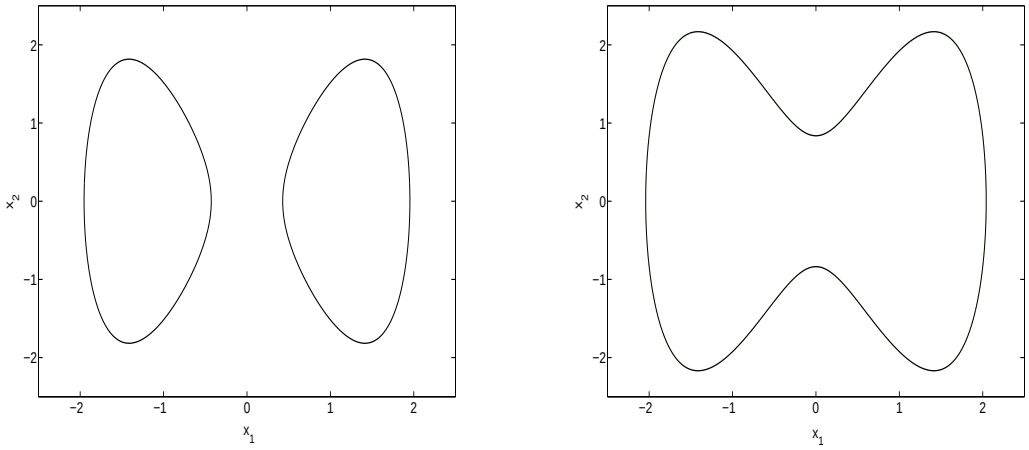

(a) Initial curve $\Gamma(0)$.

(b) $\Gamma(s)$ for some $s > 0$.

Figure 1.1: The curve $\Gamma(t)$ evolving in the direction of its outward normal vector.

Consider a system that evolves according to

$$\dot{x}(t) = f(x(t), u(t)) \quad \text{for } 0 \leq t \leq T, \tag{1.6}$$

$$x(t = 0) = x_0, \tag{1.7}$$

where $x(t) \in \mathbb{R}^n$ is the state vector at time t, $\dot{x}(t) \in \mathbb{R}^n$ is the vector of first order time derivatives of the states at time t, $u(t) \in U \subset \mathbb{R}^m$ is the control vector at time t (note that its dimension does not have to be the same as the dimension of the state vector), U is the control constraint set, and T is the terminal time. We assume that the functions $f_i, i = 1, ..., n$, are continuously differentiable with respect to x and continuous with respect to u, and that the admissible control functions (also called *control trajectories*) are the piecewise continuous functions $\{u(t) \,|\, t \in [0, T]\}$ with $u(t) \in U$ for all $t \in [0, T]$. We also assume that for any admissible control trajectory, the system of differential equations (1.6), (1.7) has a unique solution, referred to as the corresponding *state trajectory*.

We wish to find an admissible control trajectory $\{u(t) \,|\, t \in [0, T]\}$, which

together with its corresponding state trajectory minimizes a cost function of the form

$$h(x(T)) + \int_0^T g(x(t), u(t))dt, \tag{1.8}$$

where the functions h and g are continuously differentiable with respect to x and g is continuous with respect to u. The function h represents a terminal cost that is incurred at the end of the process, and g is an additive cost that accumulates over time. The dynamic programming approach involves the introduction of a function $V(x,t)$ called the *optimal cost-to-go* function, which represents the minimal cost that could be incurred if one is to begin at a state $x(t)$ at time t. Clearly, V must satisfy the boundary condition $V(x,T) = h(x(T))$.

Divide the time interval $[0,T]$ into N subintervals of length $\Delta t = T/N$, and assume that the control variable u can be changed only at times $t = k\,\Delta t$, $k = 0, 1, ..., N$. Once we find an equation satisfied by this discrete version of the optimal cost-to-go function, we can take the limit as $\Delta t \to 0$ to obtain an equation satisfied by the continuous-time optimal cost-to-go function. In the discrete-time framework, at (x,t), the optimal cost-to-go function satisfies

$$V(x(t),t) = \min_{u \in \mathbb{R}^m} \left\{ g(x,u)\Delta t + V(x(t+\Delta t), t+\Delta t) \right\}. \tag{1.9}$$

Heuristically, this says that if we are at state $x(t)$ at time t, the best we can do is to find an action (value of the control variable) that minimizes the cost in the next time interval $[t, t+\Delta t]$ and the best one can do in the future, i.e., in the interval $[t+\Delta t, T]$. Since the state trajectory $x(t)$ in the discrete-time framework satisfies

$$x(t+\Delta t) = x(t) + \Delta t\, f(x(t), u(t)),$$

(1.9) becomes

$$V(x(t),t) = \min_{u \in \mathbb{R}^m} \left\{ g(x,u)\Delta t + V(x + \Delta t\, f(x,u), t+\Delta t) \right\}.$$

Using the fact that the Taylor expansion of the term $V(x + \Delta t\, f(x,u), t + \Delta t)$ around (x,t) is

$$V(x + \Delta t\, f(x,u), t + \Delta t) = V(x,t) + V_t(x,t)\Delta t + \nabla_x V(x,t) \cdot f(x,u)\Delta t + O(\Delta t^2),$$

we obtain

$$0 = \min_{u \in \mathbb{R}^m} \left\{ g(x,u)\Delta t + V_t(x,t)\Delta t + \nabla_x V(x,t) \cdot f(x,u)\Delta t + O(\Delta t^2) \right\}.$$

Dividing both sides by Δt and taking the limit as $\Delta t \to 0$ yields

$$V_t(x,t) + \min_{u \in \mathbb{R}^m} \{ g(x,u) + \nabla_x V(x,t) \cdot f(x,u) \} = 0. \tag{1.10}$$

Together with the terminal condition $V(x,T) = h(x)$, (1.10) is the *Hamilton-Jacobi-Bellman* equation corresponding to the continuous-time dynamic system (1.6), (1.7) subject to the cost function (1.8). It can be shown that $V(x_0, 0)$ is the minimum possible cost and

$$u_{\text{opt}} = \arg \min_{u \in \mathbb{R}^m} \{ g(x,u) + \nabla_x V(x,t) \cdot f(x,u) \}$$

is the optimal control trajectory. See [5] for details and examples of Hamilton-Jacobi-Bellman equations arising in applications.

Hamilton-Jacobi-Bellman equations have also gained a wide popularity in finance since many nonlinear option pricing problems can be naturally posed as optimal control problems. Forsyth and Labahn [17] provide a brief overview of such problems including the pricing of American options, derivatives pricing models with unequal borrowing/lending rates, pricing of certain insurance products in incomplete markets, and derivatives pricing models accounting for stock borrowing fees, to name a few.

1.3 Plan for the dissertation

The remainder of the dissertation is organized as follows.

- **Chapter 2**. We introduce the definition of the semi-differentials of continuous functions and the definition of the weak solutions of time-dependent Hamilton-Jacobi equations known as the viscosity solutions. We also provide the statement and the proof of a very important theoretical result that provides a method for constructing viscosity solutions of time-dependent Hamilton-Jacobi equations.

- **Chapter 3**. We state, discuss and give the proof of the a posteriori error estimate.

- **Chapter 4**. We study the efficiency of the a posteriori error estimate on a few problems in one space dimension. We test the a posteriori estimate using approximations generated by a classic monotone scheme that is known to converge to the viscosity solutions of time-dependent Hamilton-Jacobi equations.

- **Chapter 5**. We summarize the results of this dissertation and conclude with a discussion of future directions of research.

Chapter 2

Viscosity Solutions

2.1 Definitions

In this section we recall the definition of a viscosity solution of the initial-value problem for the time-dependent first order Hamilton-Jacobi equation (1.1), (1.2). In order to define the viscosity solution of (1.1), (1.2), we need the notion of *semi-differentials* of a function defined on $\mathbb{R}^d \times (0,T)$.

The *superdifferential* of a function u at a point $(x,t) \in \mathbb{R}^d \times (0,T)$, $D^+u(x,t)$, is defined as the set of all vectors $p = (p_x, p_t) \in \mathbb{R}^d \times \mathbb{R}$ such that

$$\limsup_{(y,s)\in\mathbb{R}^d\times(0,T)\to(x,t)} \left(\frac{u(y,s) - \{u(x,t) + (s-t)\,p_t + (y-x)\cdot p_x\}}{\| (y,s) - (x,t) \|} \right) \leq 0.$$

Similarly, the *subdifferential* of a function u at a point $(x,t) \in \mathbb{R}^d \times (0,T)$, $D^-u(x,t)$, is defined as the set of all vectors $p = (p_x, p_t) \in \mathbb{R}^d \times \mathbb{R}$ such that

$$\liminf_{(y,s)\in\mathbb{R}^d\times(0,T)\to(x,t)} \left(\frac{u(y,s) - \{u(x,t) + (s-t)\,p_t + (y-x)\cdot p_x\}}{\| (y,s) - (x,t) \|} \right) \geq 0.$$

Let us denote the exact differential of a function $v \in C^1\left(\mathbb{R}^d \times (0,T)\right)$ at a point (x,t) by $Dv(x,t)$, i.e., $Dv(x,t) = (\nabla v(x,t), v_t(x,t))$. An equivalent characterization of semi-differentials is provided in the following lemma.

Lemma 2.1.1. *Let* $u \in C\left(\mathbb{R}^d \times (0,T)\right)$.

i. $p \in D^+u(x,t)$ *if and only if there exists a function* $v \in C^1\left(\mathbb{R}^d \times (0,T)\right)$ *such that* $Dv(x,t) = p$ *and* $u - v$ *has a local maximum at* (x,t).

ii. $p \in D^-u(x,t)$ *if and only if there exists a function* $v \in C^1\left(\mathbb{R}^d \times (0,T)\right)$ *such that* $Dv(x,t) = p$ *and* $u - v$ *has a local minimum at* (x,t).

Proofs of Lemma 2.1.1 can be found in [6] and [11]. Note that by replacing the function v by $\tilde{v}(y,s) = v(y,s) \pm \delta(|y-x|^2 + (s-t)^2)$ for some $\delta > 0$, it is clear that in the above lemma we can require that $u - v$ attains a *strict* local maximum or minimum at the point (x,t).

We also need to define the residual $R(x,p) = p_t + H(x,p_x)$. With the above notation, we are ready to state the definition of a viscosity solution of the initial-value problem (1.1), (1.2).

Definition 2.1.2. *A* ***viscosity solution*** *of the initial-value problem (1.1), (1.2) is a continuous function* u *in* $\mathbb{R}^d \times (0,T)$ *such that* $u(t=0) = u_0$ *and for all* $(x,t) \in \mathbb{R}^d \times (0,T)$,

$$R(x,p) \leq 0, \quad \forall p \in D^+u(x,t), \tag{2.1}$$

and

$$R(x,p) \geq 0, \quad \forall p \in D^-u(x,t). \tag{2.2}$$

If u satisfies (2.1), it is called a **viscosity subsolution** of (1.1), (1.2), and if it satisfies (2.2), it is called a **viscosity supersolution** of (1.1), (1.2). Note that we can write (2.1) and (2.2) as

$$\sigma R(x,p) \leq 0, \quad \forall p \in D^\sigma u(x,t),\ \sigma \in \{-,+\}.$$

Definition 2.1.2 is very useful for computational purposes and the a posteriori error estimate given in the next chapter is based on it. In view of Lemma 2.1.1, we can reformulate Definition 2.1.2 in the following equivalent form:

Definition 2.1.3. *A **viscosity solution** of (1.1), (1.2) is a continuous function u in $\mathbb{R}^d \times (0,T)$ such that $u(t=0) = u_0$ and for all $v \in C^1\left(\mathbb{R}^d \times (0,T)\right)$,*

$$\begin{cases} \text{if } u - v \text{ has a local maximum at a point } (x,t) \in \mathbb{R}^d \times (0,T), \text{ then} \\ v_t(x,t) + H(x, \nabla v(x,t)) \leq 0 \end{cases} \tag{2.3}$$

and

$$\begin{cases} \text{if } u - v \text{ has a local minimum at a point } (x,t) \in \mathbb{R}^d \times (0,T), \text{ then} \\ v_t(x,t) + H(x, \nabla v(x,t)) \geq 0. \end{cases} \tag{2.4}$$

u is a **viscosity subsolution** if it satisfies (2.3) and a **viscosity supersolution** if it satisfies (2.4).

2.2 Construction of viscosity solutions

When studying partial differential equations of the form (1.1), (1.2), it is natural to consider an appropriate parabolic regularization such as

$$u_t^\epsilon + H(x, \nabla u^\epsilon) = \epsilon \, \Delta u^\epsilon \quad \text{for } (x,t) \in \mathbb{R}^d \times (0,T), \tag{2.5}$$

$$u^\epsilon(x, t=0) = u_0(x) \quad \text{for } x \in \mathbb{R}^d, \tag{2.6}$$

where $\epsilon > 0$. The idea is that (2.5), (2.6) is a quasilinear parabolic partial differential equation, which has a smooth solution. We then hope that if we let $\epsilon \to 0$, the solution u^ϵ will converge to some sort of a weak solution of (1.1), (1.2). This is the *method of vanishing viscosity*.

We can show that if a solution to (1.1), (1.2) is constructed using the method of vanishing viscosity, then it indeed satisfies Definition 2.1.3.

Theorem 2.2.1. *Let u^ϵ be a family of smooth solutions to the viscous equation (2.5), (2.6). Assume that as $\epsilon \to 0$, u^ϵ converges uniformly to some $u \in C\left(\mathbb{R}^d \times (0,T)\right)$. Then u is a viscosity solution of (1.1), (1.2).*

Proof. Proofs of the theorem for general nonlinear first order partial differential equations can be found in [6] and [11]. We follow a development similar to the one given in [11].

1. Let us first show that for a test function $\varphi \in C^2\left(\mathbb{R}^d \times (0,T)\right)$, inequalities (2.3) and (2.4) hold. Assume that $u - \varphi$ has a local maximum at some point $(x_0, t_0) \in \mathbb{R}^d \times (0,T)$. Choose $\psi \in C^\infty\left(\mathbb{R}^d \times (0,T)\right)$ such that $\psi(x_0,t_0) = 1$ and $0 \le \psi(y,s) < 1$ when $(y,s) \neq (x_0,t_0)$. Then

$$\psi_t(x_0,t_0) = 0 \quad \text{and} \quad \nabla\psi(x_0,t_0) = 0. \tag{2.7}$$

It is clear that $u - (\varphi - \psi)$ has a strict local maximum at (x_0,t_0). Since $u^\epsilon \to u$ uniformly in $\mathbb{R}^d \times (0,T)$, for ϵ sufficiently small, $u^\epsilon - (\varphi - \psi)$ has a local maximum at some point $(x_\epsilon, t_\epsilon) \in \mathbb{R}^d \times (0,T)$ and $(x_\epsilon,t_\epsilon) \to (x_0,t_0)$ as $\epsilon \to 0$. Therefore,

$$\begin{aligned}
u_t^\epsilon(x_\epsilon,t_\epsilon) &= (\varphi_t - \psi_t)(x_\epsilon,t_\epsilon),\\
\nabla u^\epsilon(x_\epsilon,t_\epsilon) &= \nabla(\varphi-\psi)(x_\epsilon,t_\epsilon),\\
\Delta u^\epsilon(x_\epsilon,t_\epsilon) &\le \Delta(\varphi-\psi)(x_\epsilon,t_\epsilon),
\end{aligned}$$

which further implies that

$$\begin{aligned}
(\varphi_t - \psi_t)(x_\epsilon,t_\epsilon) + H\left(x_\epsilon, \nabla(\varphi-\psi)(x_\epsilon,t_\epsilon)\right) &= u_t^\epsilon(x_\epsilon,t_\epsilon) + H\left(x_\epsilon, \nabla u^\epsilon(x_\epsilon,t_\epsilon)\right)\\
&= \epsilon\,\Delta u^\epsilon(x_\epsilon,t_\epsilon)\\
&\le \epsilon\,\Delta(\varphi-\psi)(x_\epsilon,t_\epsilon).
\end{aligned}$$

Using (2.7) and since $(x_\epsilon,t_\epsilon) \to (x_0,t_0)$ and $\epsilon\,\Delta(\varphi-\psi)(x_\epsilon,t_\epsilon) \to 0$ as $\epsilon \to 0$, we conclude that

$$\varphi_t(x_0,t_0) + H\left(x_0, \nabla\varphi(x_0,t_0)\right) \le 0.$$

Similar arguments show that if $\varphi \in C^2\left(\mathbb{R}^d \times (0,T)\right)$ and $u-\varphi$ has a local minimum at $(x_0,t_0) \in \mathbb{R}^d \times (0,T)$, then

$$\varphi_t(x_0,t_0) + H\left(x_0, \nabla\varphi(x_0,t_0)\right) \geq 0.$$

2. Let $v \in C^1\left(\mathbb{R}^d \times (0,T)\right)$ and assume that $u-v$ has a local maximum at $(x_0,t_0) \in \mathbb{R}^d \times (0,T)$. Similarly to **1.**, choose $\psi \in C^\infty\left(\mathbb{R}^d \times (0,T)\right)$ such that $\psi(x_0,t_0) = 1$ and $0 \leq \psi(y,s) < 1$ when $(y,s) \neq (x_0,t_0)$. Clearly, $u-(v-\psi)$ has a strict local maximum at (x_0,t_0). Let $\phi_m \in C^2\left(\mathbb{R}^d \times (0,T)\right)$ be a sequence of functions such that $\phi_m \to v$ in $C^1\left(\mathbb{R}^d \times (0,T)\right)$. Then

$$u-(\phi_m-\psi) \to u-(v-\psi) \quad \text{uniformly in } \mathbb{R}^d \times (0,T),$$

and $u-(\phi_m-\psi)$ has a local maximum at a point $(x_m,t_m) \in \mathbb{R}^d \times (0,T)$ with $(x_m,t_m) \to (x_0,t_0)$. Since $\phi_m - \psi \in C^2\left(\mathbb{R}^d \times (0,T)\right)$, we can use the result from **1.** to deduce that

$$(\phi_m-\psi)_t(x_m,t_m) + H\left(x_m, \nabla(\phi_m-\psi)(x_m,t_m)\right) \leq 0.$$

Passing to the limit as $m \to \infty$ in the above inequality and using the fact that $(\phi_m)_t \to v_t$ and $\nabla\phi_m \to \nabla v$, we conclude that

$$v_t(x_0,t_0) + H\left(x_0, \nabla v(x_0,t_0)\right) \leq 0,$$

i.e., u is a viscosity subsolution of (1.1), (1.2) by Definition 2.1.3. Similar arguments can be used to show that u is also a viscosity supersolution of (1.1), (1.2). □

In the numerical experiments we use the classic Lax-Friedrichs scheme to approximate the viscosity solutions of time-dependent Hamilton-Jacobi equations [13]. It is interesting to note that the scheme is based on the idea of the vanishing viscosity method, i.e., a discrete version of the artificial viscosity term is added to the discretized Hamilton-Jacobi equation.

Chapter 3

A Posteriori Error Estimates

3.1 Derivation of the local a posteriori error estimate

Given any sub-domain Ω of $\mathbb{R}^d$ and any time $T > 0$, the local a posteriori error estimate that we propose gives an upper bound for the semi-norms

$$\begin{aligned} |\, u - v \,|_{-,\Omega,T} &= \sup_{x\in\Omega} \left(u(x,T) - v(x,T)\right)^+, \\ |\, u - v \,|_{+,\Omega,T} &= \sup_{x\in\Omega} \left(v(x,T) - u(x,T)\right)^+, \end{aligned}$$

in terms of the behavior of the function v on the set

$$Q_T = \bigcup_{t\in(0,T)} \Omega_{V(T-t)} \times \{t\},$$

where

$$\Omega_{Vt} = \{x : \ \mathrm{dist}(x,\Omega) \leq Vt\},$$

and in terms of the quantity $|\, u - v \,|_{\sigma,\Omega_{VT},0}$. The positive parameter V is defined as

$$V = \sup_{x\in\mathbb{R}^d} |\, H(x,\cdot) \,|_{\mathrm{Lip}}, \tag{3.1}$$

where the right-hand side is assumed to be finite. This ensures that if a characteristic hits the border of Q_T, it does not enter into Q_T. Moreover, Q_T is nothing but (the intersection with $\mathbb{R}^d \times (0,T)$ of) the union of the cones of dependence with vertices in Ω; see Figure 3.1 below.

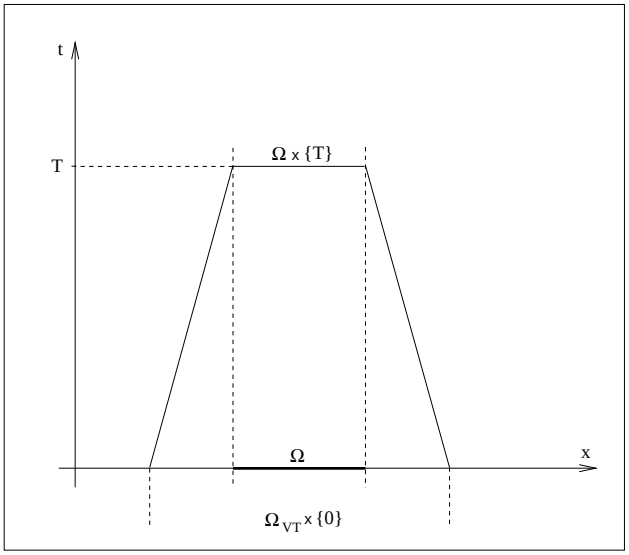

Figure 3.1: The region enclosed by the trapezoid Q_T. The viscosity solution u in $\Omega \times \{T\}$ does not depend on its initial values outside of Ω_{VT}.

In order to give the statement and the proof of the error estimate, we need to introduce the following notation. For any vector $p = (p_x, p_t) \in \mathbb{R}^d \times \mathbb{R}$ and $\epsilon = (\epsilon_x, \epsilon_t)$ with $\epsilon_x, \epsilon_t > 0$, the shifted residual R_ϵ is defined as

$$R_\epsilon(x,p) = p_t + H(x - \epsilon_x p_x, p_x). \tag{3.2}$$

For $\kappa = (\kappa_x, \kappa_t) \in \mathbb{R}^2$, the paraboloid P_v is given by

$$P_v(x,t,p,\kappa;y,s) = v(x,t) + (y-x, s-t)\cdot p + \frac{\kappa_t}{2}|\, s-t\,|^2 + \frac{\kappa_x}{2}|\, y-x\,|^2, \tag{3.3}$$

for all $(y,s) \in \mathbb{R}^d \times [0,T]$. We also need the quantity

$$\omega_\epsilon(v;x,t,p) = v(x,t) - v(x-\epsilon_x p_x, 0) - \frac{\epsilon_x}{2}|\, p_x\,|^2 - \frac{t^2}{2\epsilon_t}. \tag{3.4}$$

ω_ϵ incorporates into the estimate information about the smoothness of the function v. It can be bounded in terms of the moduli of continuity of v. For example, if $v(t=0) \in W^{1,\infty}(\mathbb{R}^d)$ and $v_t \in L^\infty(0,T;\mathbb{R}^d)$,

$$|\,\omega_{\sigma\epsilon}(v;x,t,p)\,| \leq \frac{|\,v_t\,|^2_{L^\infty(0,T;\mathbb{R}^d)}}{2}\epsilon_t + \frac{|\,v(0)\,|_{W^{1,\infty}(\mathbb{R}^d)}}{2}\epsilon_x. \tag{3.5}$$

With the notation introduced above, we have the following result.

Theorem 3.1.1. *Let u be the viscosity solution of the problem* (1.1), (1.2) *and let v be any continuous function on $\mathbb{R}^d \times [0,T]$. Let Ω be a sub-domain of $\mathbb{R}^d$. Then, for $\sigma \in \{-,+\}$, we have that*

$$|\,u-v\,|_{\sigma,\Omega,T} \leq |\,u-v\,|_{\sigma,\Omega_{VT},0} + \inf_{\epsilon_x,\epsilon_t>0} \Phi_\sigma(v;\epsilon), \tag{3.6}$$

where

$$\Phi_\sigma(v;\epsilon) = \sup_{((x,t),p)\in\mathcal{A}_\sigma(v;\epsilon)} \left\{ \big(\sigma\,\omega_{\sigma\epsilon}(v;x,t,p)\big)^+ + \big(\sigma\,T\,R_{\sigma\epsilon}(x,p)\big)^+ \right\}. \tag{3.7}$$

The set $\mathcal{A}_\sigma(v;\epsilon)$ is the set of points $((x,t),p)$ in $\overline{Q_T} \times \mathbb{R}^{d+1}$ such that

$$\sigma\left\{v(y,s) - P_v(x,t,p,(\sigma/\epsilon_x,\sigma/\epsilon_t)\,;\,y,s)\right\} \leq 0 \qquad \forall (y,s) \in \overline{Q_T}. \tag{3.8}$$

As stated in the introduction, the above estimate reduces to the global a posteriori error estimate obtained in [3] when $\Omega = \mathbb{R}^d$.

Proof of Theorem 3.1.1. The proof we present next is a modification of the one presented in [3] for the case $\Omega = \mathbb{R}^d$. We only prove the result for $\sigma = -$ since the proof for $\sigma = +$ is entirely analogous. We proceed in several steps.

Step 1: The auxiliary quantity Δ_δ. Note that Definition 2.1.2 of the viscosity solution holds only in the interior of Q_T. So instead of working with the quantity

$$\Delta = \sup_{(x,t)\in Q_T} (u(x,t)-v(x,t)) - |\,u-v\,|_{-,\Omega_{VT},0},$$

we consider the auxiliary quantity

$$\Delta_\delta = \sup_{(x,t)\in Q_T} \left(u(x,t) - v(x,t) - \frac{\delta}{\Psi(x,t)} \right) - | u - v |_{-,\Omega_{VT},0},$$

where δ is an arbitrary positive parameter,

$$\Psi(x,t) = T - t - \phi(x),$$

and the function ϕ is constructed in such a way that $\Psi(x,t) > 0$ in the interior of Q_T and that $\Psi(x,t) = 0$ for (x,t) in the set $\partial Q_T \setminus \Omega_{VT} \times \{0\}$.

It is not difficult to see that the function ϕ is nothing but the (suitably scaled) distance function to the set Ω. More precisely, ϕ is identically equal to zero in Ω, and outside Ω, it is the viscosity solution of the eikonal equation

$$\begin{aligned} V \,|\, \nabla\phi(x) \,| - 1 = 0 \qquad & \text{for } x \in \Omega^c, \\ \phi(x) = 0 \qquad & \text{for } x \in \partial\Omega. \end{aligned}$$

Clearly, for $t \in [0,T]$, we have

$$\Omega_{V(T-t)} = \{x \in \mathbb{R}^d \,|\, \Psi(x,t) > 0\}. \tag{3.9}$$

Step 2: The auxiliary quantity $\Delta_{\delta,\nu}$. In order to avoid some technical difficulties originating from the fact that ϕ may not be differentiable, we are going to replace it by a smoother function. To do so, we choose a smooth, nonnegative function η with integral equal to one and support in the unit ball and consider the function

$$\phi_\nu(x) = \eta_\nu(x) * \phi(x),$$

where $\eta_\nu(x) = \frac{1}{\nu^d}\,\eta(\frac{x}{\nu})$ for all $\nu > 0$, and $*$ denotes the convolution with respect to x. Clearly, ϕ_ν is a smooth function. Accordingly, we replace $\Psi(x,t)$ by $\Psi_\nu(x,t) = T - t - \phi_\nu(x)$.

Now, instead of considering the quantity Δ_δ, we take

$$\Delta_{\delta,\nu} = \sup_{(x,t)\in Q_{T,\nu}} \left(u(x,t) - v(x,t) - \frac{\delta}{\Psi_\nu(x,t)} \right) - |\, u - v \,|_{-,\Omega_{VT},0},$$

where

$$Q_{T,\nu} = \{(x,t) \in \mathbb{R}^d \times (0,T) \,|\, \Psi_\nu(x,t) > 0\}. \tag{3.10}$$

Note that for every $(x,t) \in Q_T$ we can write

$$u(x,t) - v(x,t) \le |\, u - v \,|_{-,\Omega_{VT},0} + \Delta_{\delta,\nu} + \frac{\delta}{\Psi_\nu(x,t)}, \tag{3.11}$$

for some $\nu < \nu_0$, $\nu_0 > 0$, because of the definitions of Q_T and $Q_{T,\nu}$, (3.9) and (3.10), and the fact that $\lim_{\nu\downarrow 0} \phi_\nu(x) = \phi(x)$ for all $x \in \mathbb{R}^d$ since ϕ is continuous.

The idea of the proof is to obtain an estimate of the form

$$\Delta_{\delta,\nu} \le C \quad \forall \delta \le \delta_0,$$

for some constants $C \ge 0$ and $\delta_0 > 0$. If we then let $\delta \to 0$ in (3.11), we obtain the desired result, namely,

$$|\, u - v \,|_{-,\Omega,T} \le |\, u - v \,|_{-,\Omega_{VT},0} + C. \tag{3.12}$$

Step 3: The auxiliary function ψ. Assume now that for some $\delta > 0$ and $\nu > 0$, $\Delta_{\delta,\nu} > 0$; otherwise, there is nothing to prove. We introduce the auxiliary function $\psi(x,t;y,s)$ defined by

$$\psi(x,t;y,s) = u(x,t) - v(y,s) - \frac{\delta}{\Psi_\nu(x,t)} - (1-\theta)\frac{(t+s)}{2\,T}\Delta_{\delta,\nu} - \frac{(t-s)^2}{2\epsilon_t} - \frac{|x-y|^2}{2\epsilon_x},$$

where $\theta \in (0,1)$ is a parameter to be determined later. Since both u and v are continuous and $Q_{T,\nu}$ is bounded, there exists a point $(\hat{x},\hat{t};\hat{y},\hat{s}) \in \overline{Q_{T,\nu}} \times \overline{Q_{T,\nu}}$ such that

$$\psi(\hat{x},\hat{t};\hat{y},\hat{s}) \ge \psi(x,t;y,s) \qquad \forall\, (x,t;y,s) \in \overline{Q_{T,\nu}} \times \overline{Q_{T,\nu}}. \tag{3.13}$$

Note that by definition of $Q_{T,\nu}$, (3.10), $\Psi_\nu(x,t) \geq 0$ for all the points $(x,t) \in \overline{Q_{T,\nu}}$. Since $\Psi_\nu(\hat{x},\hat{t})$ cannot be equal to zero, we must have that $\Psi_\nu(\hat{x},\hat{t}) > 0$. This implies that either $(\hat{x},\hat{t})$ belongs to the domain $Q_{T,\nu}$ or $\hat{t} = 0$.

Moreover, if we set

$$\hat{p} = (\hat{p}_y, \hat{p}_s) = \left(\frac{(\hat{x} - \hat{y})}{\epsilon_x}, -\frac{(1-\theta)}{2\,T}\Delta_{\delta,\nu} + \frac{(\hat{t} - \hat{s})}{\epsilon_t} \right),$$

the point $((\hat{y},\hat{s}),\hat{p})$ belongs to the set $\mathcal{A}_-(v;\epsilon)$. Indeed, taking $t = \hat{t}$ and $x = \hat{x}$ in (3.13), we obtain

$$\begin{aligned} v(y,s) &\geq v(\hat{y},\hat{s}) + \hat{p}\cdot(y-\hat{y}, s-\hat{s}) - \frac{1}{2\epsilon_t}|\, s-\hat{s}\,|^2 - \frac{1}{2\epsilon_x}|\, y-\hat{y}\,|^2 \\ &= P_v(\hat{y},\hat{s},\hat{p},(-1/\epsilon_t, -1/\epsilon_x); y, s). \end{aligned}$$

Step 4: The case $\hat{t} > 0$. Assume that $\hat{t} > 0$. In this case, since the mapping $(x,t) \mapsto \psi(x,t;\hat{y},\hat{s})$ attains a maximum at $(\hat{x},\hat{t}) \in Q_{T,\nu}$, we have that

$$\begin{aligned} 0 \in D^+_{x,t}\psi(\hat{x},\hat{t};\hat{y},\hat{s}) = D^+u(\hat{x},\hat{t}) &- \left(0, \frac{(1-\theta)}{T}\Delta_{\delta,\nu}\right) \\ &+ \frac{\delta}{\Psi^2_\nu(\hat{x},\hat{t})}\left(\nabla\Psi_\nu(\hat{x},\hat{t}), \partial_t\Psi_\nu(\hat{x},\hat{t})\right) - \hat{p}. \end{aligned}$$

Hence,

$$-\frac{\delta}{\Psi^2_\nu(\hat{x},\hat{t})}\left(\nabla\Psi_\nu(\hat{x},\hat{t}), \partial_t\Psi_\nu(\hat{x},\hat{t})\right) + \left(0, \frac{(1-\theta)}{T}\Delta_{\delta,\nu}\right) + \hat{p} \in D^+u(\hat{x},\hat{t}).$$

Since u is the viscosity solution, Definition 2.1.2 implies that

$$-\frac{\delta}{\Psi^2_\nu(\hat{x},\hat{t})}\partial_t\Psi_\nu(\hat{x},\hat{t}) + \frac{(1-\theta)}{T}\Delta_{\delta,\nu} + \hat{p}_s + H\left(\hat{x}, \hat{p}_y - \frac{\delta}{\Psi^2_\nu(\hat{x},\hat{t})}\nabla\Psi_\nu(\hat{x},\hat{t})\right) \leq 0,$$

which can be written as

$$\frac{(1-\theta)}{T}\Delta_{\delta,\nu} \leq -\hat{p}_s - H(\hat{x},\hat{p}_y) + \Theta, \tag{3.14}$$

where

$$\Theta = \frac{\delta}{\Psi_\nu^2(\hat{x},\hat{t})}\partial_t\Psi_\nu(\hat{x},\hat{t}) + H(\hat{x},\hat{p}_y) - H\left(\hat{x},\hat{p}_y - \frac{\delta}{\Psi_\nu^2(\hat{x},\hat{t})}\nabla\Psi_\nu(\hat{x},\hat{t})\right).$$

Next, we show that $\Theta \leq 0$. Indeed, by the definition of the parameter V, (3.1),

$$\Theta \leq \frac{\delta}{\Psi_\nu^2(\hat{x},\hat{t})}\partial_t\Psi_\nu(\hat{x},\hat{t}) + V\frac{\delta}{\Psi_\nu^2(\hat{x},\hat{t})}|\,\nabla\Psi_\nu(\hat{x},\hat{t})\,|.$$

Using the fact that

$$\left(\nabla\Psi_\nu(\hat{x},\hat{t}), \partial_t\Psi_\nu(\hat{x},\hat{t})\right) = \left(-\nabla\phi_\nu(\hat{x}), -1\right),$$

we obtain

$$\Theta \leq -\frac{\delta}{\Psi_\nu^2(\hat{x},\hat{t})}\left(1 - V|\,\nabla\phi_\nu(\hat{x})\,|\right).$$

Since

$$V\,|\,\nabla\phi_\nu(x)\,| \leq 1 \qquad \forall\, x \in \mathbb{R}^d, \tag{3.15}$$

we conclude that $\Theta \leq 0$. To see that the above inequality holds, it suffices to realize that the definition of ϕ implies that $\nabla\phi = 0$ in Ω, and that outside Ω, ϕ is $1/V$ times the distance-to-Ω function. This implies that all the elements p of its superdifferential and subdifferential yield $V\,|\,p\,| \leq 1$. Inequality (3.15) is a reflection of this simple fact.

Since $\Delta_{\delta,\nu} > 0$ and $\hat{x} = \hat{y} + \epsilon_x\hat{p}_y$, using (3.14) we obtain

$$\Delta_{\delta,\nu} \leq \frac{T}{1-\theta}\left(-\hat{p}_s - H(\hat{y} + \epsilon_x\hat{p}_y, \hat{p}_y)\right)^+,$$

which implies that

$$\Delta_{\delta,\nu} \leq \frac{T}{1-\theta}\left(-R_{-\epsilon}(\hat{y},\hat{p})\right)^+. \tag{3.16}$$

Step 5: The case $\hat{t} = 0$. Now, let us consider the case in which $\hat{t} = 0$. Since $\Delta_{\delta,\nu} > 0$, $1 - \theta > 0$ and $0 \leq t/T < 1$,

$$\begin{aligned}\sup_{(x,t)\in Q_{T,\nu}} \psi(x,t;x,t) &\geq \sup_{(x,t)\in Q_{T,\nu}} \left(u(x,t) - v(x,t) - \frac{\delta}{\Psi_\nu(x,t)} \right) - (1-\theta)\,\Delta_{\delta,\nu} \\ &= \Delta_{\delta,\nu} + |\,u - v\,|_{-,\Omega_{VT},0} - (1-\theta)\,\Delta_{\delta,\nu} \\ &= \theta\,\Delta_{\delta,\nu} + |\,u - v\,|_{-,\Omega_{VT},0}.\end{aligned}$$

Therefore,

$$\begin{aligned}\theta\,\Delta_{\delta,\nu} + |\,u - v\,|_{-,\Omega_{VT},0} &\leq \psi(\hat{x},0;\hat{y},\hat{s}) \\ &\leq u(\hat{x},0) - v(\hat{y},\hat{s}) - \frac{\hat{s}^2}{2\epsilon_t} - \frac{|\hat{x}-\hat{y}|^2}{2\epsilon_x} \\ &\leq |\,u - v\,|_{-,\Omega,0} + v(\hat{x},0) - v(\hat{y},\hat{s}) - \frac{\hat{s}^2}{2\epsilon_t} - \frac{|\hat{x}-\hat{y}|^2}{2\epsilon_x},\end{aligned}$$

and finally, since $\Delta_{\delta,\nu} > 0$, $\hat{x} = \hat{y} + \epsilon_x\,\hat{p}_y$ and $|\,u - v\,|_{-,\Omega,0} \leq |\,u - v\,|_{-,\Omega_{VT},0}$, we obtain

$$\Delta_{\delta,\nu} \leq \frac{1}{\theta}\left(-\omega_{-\epsilon}(v;\hat{y},\hat{s},\hat{p})\right)^+. \tag{3.17}$$

Step 6: Conclusion. Putting together the bounds (3.16) and (3.17) yields

$$\Delta_{\delta,\nu} \leq \max\left\{ \frac{A}{\theta}, \frac{B}{1-\theta} \right\},$$

where

$$A = \left(-\omega_{-\epsilon}(v;\hat{s},\hat{y},\hat{p})\right)^+ \quad \text{and} \quad B = T\,\left(-R_{-\epsilon}(\hat{y},\hat{p})\right)^+.$$

Now, we easily see that

$$\Delta_{\delta,\nu} \leq A + B,$$

by taking the limit as θ tends to $A/(A+B) \in [0,1]$. This implies that (3.12) holds with $C = A + B$ and Theorem 3.1.1 follows. □

3.2 Remarks

Remark 1. Note that since

$$\max_{\sigma=\{-,+\}} |\, h \,|_{\sigma,\Omega,T} = \| \, h(x,T) \, \|_{L^\infty(\Omega)},$$

from the estimates of the semi-norms $|\, u - v \,|_{\sigma,\Omega,T}$, we obtain

$$\| \, u(x,T) - v(x,T) \, \|_{L^\infty(\Omega)} \leq \| \, u(x,0) - v(x,0) \, \|_{L^\infty(\Omega_{VT})} + \max_{\sigma\in\{-,+\}} \inf_{\epsilon_x,\epsilon_t>0} \Phi_\sigma(v;\epsilon).$$

When v satisfies certain smoothness conditions, such as the conditions required for (3.5) to hold or v is Lipschitz in both variables, we can let ϵ_x and ϵ_t go to zero in (3.6) and using (3.5), we obtain

$$|\, u - v \,|_{\sigma,\Omega,T} \leq |\, u - v \,|_{\sigma,\Omega_{VT},0} + \sup_{((x,t),p)\in\overline{Q_T}\times D^\sigma v(x,t)} \left(\sigma \, T \, R(x,p)\right)^+,$$

which furthermore implies that

$$\begin{aligned} \| \, u(x,T) - v(x,T) \, \|_{L^\infty(\Omega)} \leq{}& \| \, u(x,0) - v(x,0) \, \|_{L^\infty(\Omega_{VT})} \\ &+ \max_{\sigma\in\{-,+\}} \left\{ \sup_{((x,t),p)\in\overline{Q_T}\times D^\sigma v(x,t)} \left(\sigma \, T \, R(x,p)\right)^+ \right\}. \end{aligned}$$

This estimate is sharp when the viscosity solution u is smooth and v has a non-oscillatory residual, as will be seen from the numerical experiments. However, for a nonsmooth viscosity solution u, the right-hand side of the above inequality might remain of order one while v converges to the viscosity solution [2].

Remark 2. The point $((x,t),p)$ belongs to the set $A_-(v;\epsilon)$ if the graph of v remains above the paraboloid $P_v(x,t,p,(-1/\epsilon_x,-1/\epsilon_t);\cdot,\cdot)$. Since the paraboloid touches v at (x,t), when (x,t) is in the interior of Q_T, p belongs to $D^- v(x,t)$. This so-called **paraboloid test**, i.e., testing whether $((x,t),p)$ belongs to $A_\sigma(v;\epsilon)$, can

be used to detect the location of the discontinuities in the gradient of the exact solution u at any time $t \in [0, T]$. Consider a viscosity solution u that has a kink at the point (x_0, t_0), for example. Let v be a smooth function that is, roughly speaking, 'very close' to the viscosity solution u. For a given value of the auxiliary parameter $\epsilon = (\epsilon_x, \epsilon_t)$, there is an interval around (x_0, t_0) such that the points inside this interval fail the paraboloid test. We illustrate this fact when we discuss the results of our numerical experiments for nonsmooth viscosity solutions.

Remark 3. We also want to stress the role played by the auxiliary parameter $\epsilon = (\epsilon_x, \epsilon_t)$. The set $A_\sigma(v; \epsilon)$ decreases as each of the components of the auxiliary parameter ϵ increases. This induces a tendency on $\Phi_\sigma(v; \epsilon)$ to decrease. At the same time, the shifted residual $\sigma R_{\sigma\epsilon}(x, p)$ might increase. The optimal value of ϵ is obtained by balancing these two tendencies.

Remark 4. From the theory of characteristics we know that the region enclosed by the trapezoid Q_T is larger than the smallest compact domain that contains the characteristics of the initial-value problem (1.1), (1.2) that enter into Ω at time T or prior to time T have entered into a shock that is inside Ω at time T. We denote this compact domain by $\Gamma_{\Omega,T}$. It is evident from equations (3.7) and (3.8) that the larger the region enclosed by the trapezoid Q_T, the larger the error estimate. This is especially true in the case when the viscosity solution is smooth inside Ω, but the trapezoid Q_T contains a part of the path of the kink in the viscosity solution, as would be illustrated by the numerical experiments. Since the viscosity solution in Ω at time T is completely determined by the initial condition in the domain of dependence of Ω and its behavior along the characteristics that enter into Ω at time T, a sharper error estimate could be obtained if we replace the trapezoid Q_T

by a smaller compact domain that better approximates $\Gamma_{\Omega,T}$.

Below we describe a practical way to determine $\Gamma_{\Omega,T}$, which can be easily implemented numerically. The idea is as follows. Assume that the Hamiltonian function $H(x,p)$ is differentiable with respect to p, and assume that the viscosity solution u of the initial-value problem (1.1), (1.2) has a gradient at all points $(x,t) \in \mathbb{R}^d \times (0,T)$. Now, let $\varphi(x,t)$ be the solution to the terminal-value problem

$$\varphi_t + \nabla_p H(x, \nabla u) \cdot \nabla \varphi = 0 \quad \text{for } (x,t) \in \mathbb{R}^d \times (0,T), \tag{3.18}$$

$$\varphi(x,T) = \begin{cases} 1 & \text{for } x \in \Omega, \\ 0 & \text{for } x \notin \Omega. \end{cases}$$

It is easily seen that the characteristics of (3.18) are also characteristics of (1.1) for $t \in [0,T]$. The solution to (3.18) is equal to 0 along the characteristics that are outside Ω at time T and is equal to 1 along the characteristics inside the domain $\Gamma_{\Omega,T}$. Since u is not known a priori, when we apply this approach to determine $\Gamma_{\Omega,T}$, we replace u by an approximation v obtained using a numerical scheme such as the Lax-Friedrichs scheme [13]. Then, we solve (3.18) numerically to obtain an approximate solution φ_h and approximate $\Gamma_{\Omega,T}$ by the domain where φ_h is nonzero; see Section 4.6 for more details.

Chapter 4

Numerical Experiments

The purpose of this chapter is to study the application of the a posteriori error estimates to approximations generated through numerical schemes; we consider a standard monotone scheme. We study the sharpness of the a posteriori error estimates for this scheme on several prototypical one-dimensional problems. Since the a posterori error estimates give upper bounds for the L^∞-norm of the difference between the viscosity solution u and any approximation v, we study how close to 1 is the so-called *effectivity index*, which is defined as

$$ei(u,v) = \frac{\Phi(v;T,\Omega)}{\| u(x,T) - v(x,T) \|_{L^\infty(\Omega)}}, \tag{4.1}$$

where Ω is an arbitrary sub-domain of $\mathbb{R}^d$. In the case when $\Omega = \mathbb{R}^d$ or $\Omega = \Omega^{per}$, where Ω^{per} is a sub-domain of $\mathbb{R}^d$ that is equal in size to the period of the viscosity solution u whenever u is periodic, we obtain the *effectivity index* for the global a posteriori error estimate. To ease the notation we use $\mathcal{D}$ to denote the domain over which we estimate the a posteriori error estimates, i.e., $\mathcal{D} = Q_T$ in the case of the local a posteriori error estimate with the trapezoid as the domain, $\mathcal{D} = \Gamma_{\Omega,T}$ in the case of the local estimate with Q_T replaced by $\Gamma_{\Omega,T}$ as explained in the

previous chapter, and $\mathcal{D} = \mathbb{R}^d \times (0, T)$ in the case of the global a posteriori error estimate. For the sake of simplicity, we use uniform grids in all our experiments.

4.1 Discretization of the norms and the nonlinear functionals of the a posteriori error estimates

Since the approximate solutions are defined by a finite number of degrees of freedom, we replace the domain $\mathcal{D}$ over which we evaluate the functionals $\Phi_\sigma(\cdot;\cdot,\cdot)$ by a finite number of points inside $\mathcal{D}$ which we denote by $\mathcal{D}_h$. We also replace the domain $\Omega \times \{T\}$ over which we evaluate the L^∞-norm of the difference between the viscosity solution u and its approximation v by a finite set of points in $\Omega \times \{T\}$ that we denote by $\Omega_{h,T}$.

Theoretically, the evaluation of the error estimates requires optimization over the set $\epsilon_x, \epsilon_t \in [0, \infty)$. In practice, however, it is sensible to replace $[0, \infty)$ with the set

$$\mathcal{E}_h = \{(\epsilon_x, \epsilon_t) = i \cdot (\omega_x/2, \omega_t/2)\,, 0 \le i \le 4\,|\ln(1/\omega_x)\,|\}\,, \tag{4.2}$$

where ω_x, given by (4.9), is an upper bound for the artificial diffusion coefficient of the numerical scheme under consideration, and ω_t is given by

$$\omega_t = \frac{\omega_x}{\Delta x}\,\Delta t.$$

We denote by $\Phi_{h,\sigma}(\cdot)$ the functionals in the a posteriori error estimates obtained after the above mentioned modifications. To simplify the notation, we also let

$$\Phi_h(v) = \max_{\sigma \in \{-,+\}} \Phi_{h,\sigma}(v).$$

The effectivity index $ei(u,v)$ is accordingly replaced by the *computational effectivity index*

$$ei_h(u,v) = \frac{\Phi_h(v)}{\| u - v \|_{L^\infty(\Omega_{h,T})}}.$$

4.2 Evaluation of the shifted residual on ∂Q_T

Note that if (x,t) is a point on ∂Q_T, the paraboloid test could be satisfied by vectors $p = (p_x, p_t) \in \mathbb{R}^d \times \mathbb{R}$ that are not necessarily in the semi-differentials of v at (x,t), making the evaluation of the shifted residual a nontrivial matter. Consider the case when $\sigma = -$. Recall that the set $\mathcal{A}_-(v;\epsilon)$ is the set of points $((x,t),p) \in \overline{Q_T} \times \mathbb{R}^{d+1}$ such that

$$v(y,s) \geq v(x,t) + p \cdot (y-x, s-t) - \frac{|\, s-t \,|^2}{2\epsilon_t} - \frac{|\, y-x \,|^2}{2\epsilon_x} \quad \forall (y,s) \in \overline{Q_T},$$

which implies that

$$\liminf_{(y,s)\to(x,t)} \frac{v(y,s) - v(x,t) - p \cdot (y-x, s-t)}{\|(y,s)-(x,t)\|} \geq 0 \quad \forall (y,x) \in \overline{Q_T}. \tag{4.3}$$

Let

$$\nu = \frac{(y,s)-(x,t)}{\|(y,s)-(x,t)\|}.$$

For simplicity assume that v is continuously differentiable in a neighborhood of the point (x,t), as is the case in many practical applications. In this case the two semi-differentials reduce to the exact differential of v and (4.3) implies that

$$(Dv(x,t) - p) \cdot \nu \geq 0, \tag{4.4}$$

which we can write as $\delta \cdot \nu \geq 0$ where $\delta = (Dv(x,t) - p)$. In particular, (4.4) holds for all ν that are inward normal to the boundary of the trapezoid ∂Q_T. Next, we show that in the case when H is a function of p only, as is the case in all our test

problems, when we compute the a posteriori error estimate, the shifted residual needs to be evaluated not at all points $((x,t),p)$ that pass the paraboloid test, but only at the points $((x,t), Dv(x,t))$. Indeed, assuming that H is differentiable in x and p, in (3.7) the term $(-R_{-\epsilon}(x,p))^+$ satisfies

$$\begin{aligned}(-R_{-\epsilon}(x,p))^+ &= (-\left[p_t + H(x+\epsilon_x p_x, p_x)\right])^+ \\ &= (-\left[v_t(x,t) + H(x+\epsilon_x \nabla v(x,t), \nabla v(x,t))\right] + \Upsilon)^+ \\ &\leq (-R_{-\epsilon}(x, \nabla v(x,t)))^+ + \Upsilon^+,\end{aligned}$$

where

$$\begin{aligned}\Upsilon =& -\delta_t - H\left(x+\epsilon_x(\nabla v(x,t)+\delta_x), \nabla v(x,t)+\delta_x\right) + H\left(x+\epsilon_x \nabla v(x,t), \nabla v(x,t)\right) \\ =& -\delta_t - \int_0^1 \frac{d}{d\eta} H\left(x+\epsilon_x(\nabla v(x,t)+\eta\,\delta_x), \nabla v(x,t)+\eta\,\delta_x\right) d\eta \\ =& -\delta_t - \int_0^1 \delta_x \cdot \epsilon_x\, \partial_x H\left(x+\epsilon_x(\nabla v(x,t)+\eta\,\delta_x), \nabla v(x,t)+\eta\,\delta_x\right) d\eta \\ & - \int_0^1 \delta_x \cdot \partial_p H\left(x+\epsilon_x(\nabla v(x,t)+\eta\,\delta_x), \nabla v(x,t)+\eta\,\delta_x\right) d\eta.\end{aligned}$$

In the case when H is a differentiable function of p only, Υ reduces to

$$\begin{aligned}\Upsilon &= -\delta \cdot \left(1, \int_0^1 \partial_p H\left(x+\epsilon_x(\nabla v(x,t)+\eta\,\delta_x), \nabla v(x,t)+\eta\,\delta_x\right) d\eta\right) \\ &\leq 0,\end{aligned}$$

where in the second inequality we have used (4.4) and the definition of the boundary of Q_T. Therefore, $(-R_{-\epsilon}(x,p))^+$ is bounded above by $(-R_{-\epsilon}(x, \nabla v(x,t)))^+$.

4.3 Fast evaluation of the paraboloid test

To evaluate the paraboloid test (3.8) is computationally very expensive. To determine if the point $((x,t),p) \in \mathcal{D} \times \mathbb{R}^{d+1}$ belongs to the set $\mathcal{A}_\sigma(v;\epsilon)$, for example, we

must compare $P_v(x,t,p,(\sigma/\epsilon_x,\sigma/\epsilon_t)\,;\,y,s)$ and $v(y,s)$ for each point $(y,s)\in\mathcal{D}$. When v is Lipschitz, however, which is the case in most practical applications, it is not necessary to perform this comparison for all (y,s) in the domain $\mathcal{D}$, but only on a significantly smaller set. Note that if P_v is 'tangent' to v at the point (y,s), we must have that

$$q=(q_x,q_t)=\left(p_x+\frac{\sigma}{\epsilon_x}(y-x),p_t+\frac{\sigma}{\epsilon_t}(s-t)\right)$$

for some $q\in D^\sigma v(y,s)$. This implies that

$$|\,y-x\,|=|\,p_x-q_x\,|\epsilon_x\le 2\epsilon_x\|\,v(\cdot,s)\,\|_{\mathrm{Lip}(\mathcal{D}_{\cdot,s})} \tag{4.5}$$

and

$$|\,s-t\,|=|\,p_t-q_t\,|\epsilon_t\le 2\epsilon_t\|\,v(y,\cdot)\,\|_{\mathrm{Lip}(\mathcal{D}_{y,\cdot})}, \tag{4.6}$$

where $\mathcal{D}_{\cdot,s}=\left\{y\in\mathbb{R}^d\,|\,(y,s)\in\mathcal{D}\right\}$ and $\mathcal{D}_{y,\cdot}=\{s\in(0,T)\,|\,(y,s)\in\mathcal{D}\}$. Thus, we can replace (3.8) by the following condition:

$$\sigma\left\{v(y,s)-P_v(x,t,p,(\sigma/\epsilon_x,\sigma/\epsilon_t)\,;\,y,s)\right\}\le 0\qquad\forall(y,s)\in\mathcal{D}:\text{(4.5), (4.6) hold.}$$

In our computations, we actually use a discrete version of the above paraboloid test, which is carried out only for (x,t), $(y,s)\in\mathcal{D}_h$.

4.4 Test problems

To study the efficiency of the global and local a posteriori error estimates, we consider the model problem

$$\begin{aligned}
&u_t+H\,(u_x)=0 && \text{for } (x,t)\in[-1,1]\times(0,\infty), \\
&u(-1,t)=u(1,t) && \text{for } t\in[0,\infty), \\
&u(x,0)=u_0(x) && \text{for } x\in[-1,1],
\end{aligned} \tag{4.7}$$

with different Hamiltonian functions and initial conditions. Our test problems involve three different Hamiltonians; a linear, a convex, and a nonconvex function. With the notation that we introduced above, $\Omega^{per} = [-1, 1]$. Table 4.1 summarizes the Hamiltonian functions $H(p)$, the initial conditions $u_0(x)$, the time intervals of consideration, and the smoothness of the viscosity solutions u at time T.

Table 4.1: Test problems.

Problem	$H(p)$	$u_0(x)$	$[0, T]$	$u(x, T)$
(L1)	$0.75p$	$\sin(\pi x)$	$[0, 0.15]$	smooth
(L2)	$0.75p$	$\begin{cases} 1 + \sin(0.5\pi x), & x \in [-1, 0] \\ 0.5 + 0.5\cos(\pi x), & x \in (0, 1] \end{cases}$	$[0, 0.15]$	nonsmooth
(C)	$0.5(p+1)^2$	$-\cos(\pi x)/\pi$	$[0, 0.20]$ $[0, 0.40]$	smooth nonsmooth
(NC)	$-\cos(p+1)$	$-\cos(\pi x)$	$[0, 0.5/\pi^2]$ $[0, 1.5/\pi^2]$	smooth nonsmooth

Note that problems (L1) and (L2), for which the Hamiltonian is a linear function, are examples of one-dimensional transport equations with constant coefficients. Their exact solutions are given by

$$u(x, t) = u_0 \left(x - 0.75t\right).$$

Figure 4.1(a)-(b) shows the exact solutions of problems (L1) and (L2) at time $T = 0.15$.

Furthermore, note that the spatial derivative of the viscosity solution of a first order one-dimensional Hamilton-Jacobi equation solves a corresponding conservation law. If we make the change of variables $\phi = u_x + 1$ in problem (4.7), we

obtain the conservation law

$$\phi_t + [H(\phi - 1)]_x = 0 \qquad \text{for } (x,t) \in [-1,1] \times (0,\infty).$$

The conservation law corresponding to test problem (C) is the well-known inviscid Burgers' equation

$$\phi_t + \phi\,\phi_x = 0,$$

and the conservation law corresponding to test problem (NC) is

$$\phi_t + \sin(\phi)\phi_x = 0.$$

We can use the theory of characteristics and shock fitting [28] to obtain information about the shocks of the corresponding conservation laws. In this way we can find the location of the kinks in the viscosity solutions of our test problems at any time t. Figure 4.1(c)-(d) shows the viscosity solution of problem (C) at time $T = 0.20$, when it is smooth, and at time $T = 0.40$, when it is nonsmooth. Similarly, Figure 4.1(e)-(f) shows the viscosity solutions of problem (NC) at times $T = 0.5/\pi^2$ and $T = 1.5/\pi^2$.

4.5 The monotone scheme

In our numerical experiments we use a monotone scheme on a uniform grid. Given the mesh sizes Δx, $\Delta t > 0$, the value of our numerical approximation to the viscosity solution u of (4.7) at $(x_j, t_n) = (j\Delta x, n\Delta t)$, $j, n \in \mathbb{Z}$, will be denoted by v_j^n. We use the following scheme

$$v_j^{n+1} = v_j^n - \Delta t \left[H\left(\frac{v_{j+1}^n - v_{j-1}^n}{2\Delta x} \right) - \frac{\theta}{\lambda} \left(\frac{v_{j+1}^n - 2v_j^n + v_{j-1}^n}{\Delta x} \right) \right], \tag{4.8}$$

where $\theta > 0$ is given and $\lambda = \Delta t/\Delta x$. This scheme is monotone as long as $1 - 2\theta \geq 0$ (monotonicity in v_j^n), and $\theta - \lambda |\, H'(\alpha)\,|/2 \geq 0$ for $\alpha \in \mathbb{R}$ (monotonicity

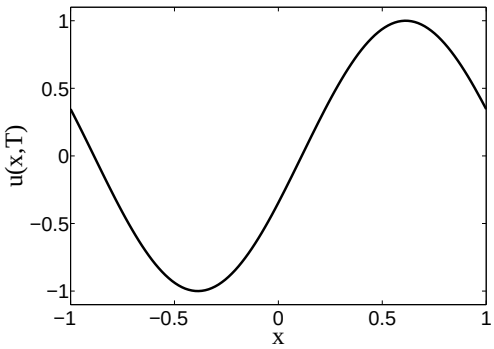

(a) Problem (L1); $T = 0.15$.

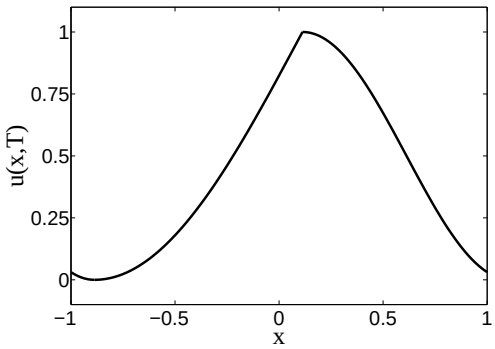

(b) Problem (L2); $T = 0.15$.

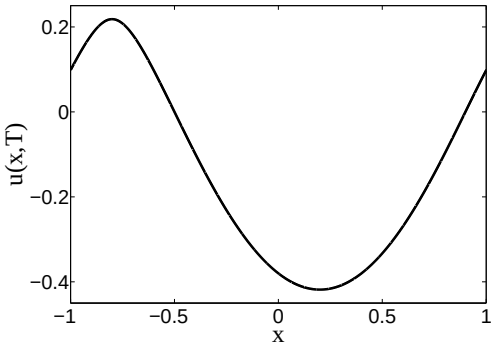

(c) Problem (C); $T = 0.20$.

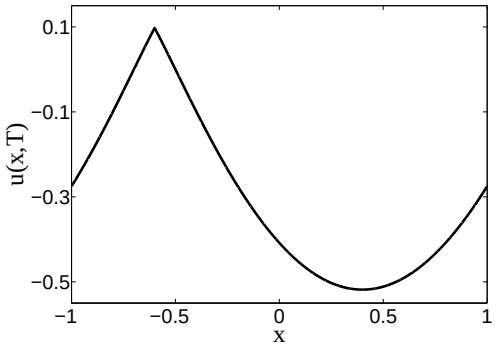

(d) Problem (C); $T = 0.40$.

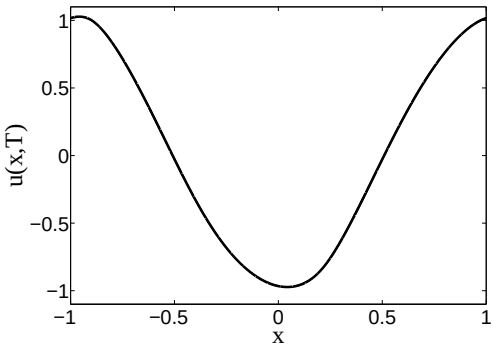

(e) Problem (NC); $T = 0.5/\pi^2$.

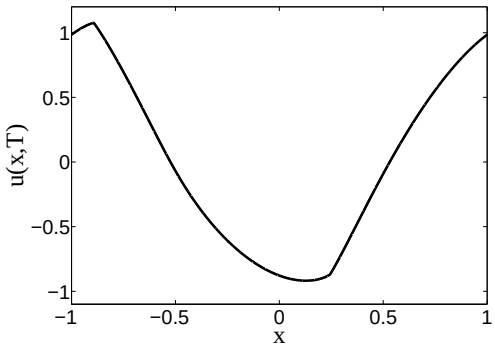

(f) Problem (NC); $T = 1.5/\pi^2$.

Figure 4.1: Exact solutions of the test problems.

in v_{j+1}^n and v_{j-1}^n) [13]. In equation (4.8), we take

$$\theta = \lambda \sup_{\alpha \in \mathbb{R}} \frac{|\, H'(\alpha)\,|}{2},$$

and fix λ in such a way that $1 - 2\theta \geq 0$ holds. This choice of θ yields the well-known Lax-Friedrichs scheme. The use of the scheme (4.8) is justified by the fact that it is guaranteed to converge to the correct viscosity solution [13]. Its downside is that it is at most first order accurate. If we let

$$\omega_x = \sup_{\alpha \in \mathbb{R}} \frac{|\, H'(\alpha)\,|}{2} \Delta x, \tag{4.9}$$

we can rewrite (4.8) as

$$\frac{v_j^{n+1} - v_j^n}{\Delta t} + H\left(\frac{v_{j+1}^n - v_{j-1}^n}{2\Delta x}\right) = \omega_x \left(\frac{v_{j+1}^n - 2v_j^n + v_{j-1}^n}{\Delta x^2}\right),$$

which is a discretized version of the Hamilton-Jacobi equation with an artificial viscosity term added, and ω_x allows the artificial viscosity to scale with the discretization.

The a posteriori error estimate (3.6) is based on the notion of viscosity solutions and so requires the comparison between continuous functions. We choose v to be the piecewise bilinear interpolant of the numerical solution given by the above scheme at the points (x_j, t_n). We then sample at the points $(x_{j+1/2}, t_{n+1/2})$, where $x_{j+1/2} = (x_{j+1} + x_j)/2$ and $t_{n+1/2} = (t_{n+1} + t_n)/2$. At the points $(x_{j+1/2}, t_{n+1/2})$ we have

$$\begin{aligned}
v(x_{j+1/2}, t_{n+1/2}) &= \frac{1}{4}\left(v_{j+1}^{n+1} + v_j^{n+1} + v_{j+1}^n + v_j^n\right), \\
v_x(x_{j+1/2}, t_{n+1/2}) &= \frac{1}{2\Delta x}\left(v_{j+1}^{n+1} - v_j^{n+1} + v_{j+1}^n - v_j^n\right), \\
v_t(x_{j+1/2}, t_{n+1/2}) &= \frac{1}{2\Delta t}\left(v_{j+1}^{n+1} - v_{j+1}^n + v_j^{n+1} - v_j^n\right).
\end{aligned}$$

Choosing the computational domain $\mathcal{D}_h$ as the sets of points $(x_{j+1/2}, t_{n+1/2})$ that lie inside $\mathcal{D}$, i.e., defining $\mathcal{D}_h$ as

$$\mathcal{D}_h = \left\{(x_{j+1/2}, t_{n+1/2}) \text{ for } j, n \in \mathbb{Z} \,|\, (x_{j+1/2}, t_{n+1/2}) \in \mathcal{D}\right\}$$

leads to well-defined derivatives of v at the points where the solution is sampled. Hence, at these points the semi-differentials are both non-empty, and $p = (p_x, p_t)$ is exactly the differential of v, i.e.,

$$D^- v(x_{j+1/2}, t_{n+1/2}) = D^+ v(x_{j+1/2}, t_{n+1/2}) = (v_x, v_t)\,(x_{j+1/2}, t_{n+1/2}).$$

As the computational domain $\Omega_{h,T}$ over which we evaluate the L^∞-norm of the difference between the viscosity solution u and the approximation v when we calculate the effectivity index, we take the union of the sets of points $\{(x_j, T) \mid x_j \in \Omega\}$ and $\left\{(x_{j+1/2}, T) \mid x_{j+1/2} \in \Omega\right\}$.

Note that calculating the upper bound for the artificial diffusion coefficient ω_x in the monotone scheme involves finding the supremum of $|\, H'(\alpha)\,|$ over all $\alpha \in \mathbb{R}$. It is easily seen that for problems (L1)-(L2) and (NC), $\sup_{\alpha\in\mathbb{R}} |\, H'(\alpha)\,|$ is equal to 0.75 and 1, respectively. For problem (C), however, $\sup_{\alpha\in\mathbb{R}} |\, H'(\alpha)\,|$ is not finite. In this case, we take

$$\omega_x = \sup_{x\in\mathbb{R}} \frac{|\, H'\left(u_0'(x)\right)\,|}{2} \Delta x = \Delta x.$$

In the numerical experiments we obtain $|\, H'\left(v_x\left(x_{j+1/2}, t_{n+1/2}\right)\right)\,| < 2$ for all the points from the computational domain, so that the monotonicity condition is preserved and the above choice for w_x is justified.

Also, recall that in one space dimension, the parameter V used in the determination of the region enclosed by the trapezoid Q_T is given by

$$V = \sup_{\substack{p_x, q_x \in \mathbb{R} \\ p_x \neq q_x}} \frac{|\, H(p_x) - H(q_x)\,|}{|\, p_x - q_x\,|},$$

where the right-hand side is assumed to be finite. V is equal to 1 and 0.75 for problems (L1)-(L2) and (NC), respectively. In the numerical experiments for problem (C) we take

$$V = \sup_{(x_{j+1/2},t_{n+1/2})\in\mathcal{D}_h^{per}} | H'\left(v_x\left(x_{j+1/2},t_{n+1/2}\right)\right) |,$$

where $\mathcal{D}_h^{per}$ is the set of points $(x_{j+1/2},t_{n+1/2})$ that lie inside $\Omega^{per}\times(0,T)$, i.e.,

$$\mathcal{D}_h^{per} = \left\{(x_{j+1/2},t_{n+1/2}) \text{ for } j,n\in\mathbb{Z} \,|\, (x_{j+1/2},t_{n+1/2})\in\Omega^{per}\times(0,T)\right\}.$$

4.6 Approximation of the domain $\Gamma_{\Omega,T}$

In this section we present the numerical implementation of the method we propose in Chapter 3 for obtaining an approximation of the smallest compact domain that contains the characteristics of the initial-value problem (1.1), (1.2) that enter into Ω at time T or prior to time T have entered into a shock that is inside Ω at time T.

Consider the terminal-value problem

$$\begin{aligned} &\phi_t + H'(u_x)\,\phi_x = 0 \qquad && \text{for } (x,t)\in\mathbb{R}\times(0,T), \\ &\phi(x,T) = \begin{cases} 1 & \text{for } x\in\Omega, \\ 0 & \text{for } x\notin\Omega, \end{cases} \end{aligned} \tag{4.10}$$

where $\Omega\in\mathbb{R}$ and u is the viscosity solution of the model initial-value Cauchy problem

$$\begin{aligned} &u_t + H(u_x) = 0 \qquad && \text{for } (x,t)\in\mathbb{R}\times(0,T), \\ &u(x,t=0) = u_0(x) \qquad && \text{for } x\in\mathbb{R}. \end{aligned} \tag{4.11}$$

We solve (4.10) backwards using a monotone scheme on the computational domain $\mathcal{D}_h^{per}$ that we described above. To simplify the notation, let $y_j := x_{j+1/2}$

and $s_n := t_{n+1/2}$. The numerical approximation to the solution of (4.10) at the points (y_j, s_n) will be denoted by $\phi_h(y_j, s_n)$ or ϕ_j^n. The monotone scheme that we use to solve (4.10) is

$$\phi_j^n = \phi_j^{n+1} + \Delta t \left[H'\left(v_x\left(y_j, s_{n+1}\right)\right) \frac{\phi_{j+1}^{n+1} - \phi_{j-1}^{n+1}}{2\Delta x} + \omega_\phi \frac{\phi_{j+1}^{n+1} - 2\phi_j^{n+1} + \phi_{j-1}^{n+1}}{\Delta x^2} \right],$$

where v is the approximation to the viscosity solution of (4.11) described in the previous section and

$$\omega_\phi = \sup_{(y_j, s_n) \in \mathcal{D}_h^{per}} \frac{|\, H'\left(v_x\left(y_j, s_n\right)\right) \,|}{2} \Delta x.$$

The monotone scheme adds an artificial diffusion term to equation (4.10), which causes the numerical approximation to $\phi(x,t)$ to be nonzero in a domain that is larger than the domain $\Gamma_{\Omega,T}$. To illustrate the effect of the artificial diffusion term with a simpler example, consider the equation

$$\rho_t = 0 \qquad \text{for } (x,t) \in \mathbb{R} \times (0,T), \tag{4.12}$$

with the terminal condition

$$\rho(x,T) = \begin{cases} 1 & \text{for } x \leq 0, \\ 0 & \text{for } x > 0. \end{cases}$$

Trivially, the solution is $\rho(x,t) = \rho(x,T)$ for all $t \in (0,T)$. For $\kappa > 0$, the solution to

$$\rho_t^d = \kappa \rho_{xx}^d \qquad \text{for } (x,t) \in \mathbb{R} \times (0,T), \tag{4.13}$$

with the same terminal condition, however, is given by

$$\rho^d(x,t) = \frac{1}{2} - \frac{1}{2} \operatorname{Erf}\left(\frac{x}{\sqrt{4\kappa(T-t)}} \right),$$

where

$$\mathrm{Erf(x)} = \frac{2}{\sqrt{\pi}} \int_0^x e^{-p^2} dp.$$

Thus, the solution to the equation with the added diffusion term is monotonically decreasing and nonzero for all $-\infty < x < \infty$. Therefore, if we want to approximate the sub-domain of $\mathbb{R}$, in which the solution to (4.12) is nonzero by considering the solution to (4.13), we have to ignore the sub-domain of $\mathbb{R}$, in which the solution to (4.13) is 'relatively' small.

We define our approximation to the domain $\Gamma_{\Omega,T}$ in a similar fashion. Let us denote this approximation by $\Gamma_{h,\Omega,T}$. At each time level n of $\mathcal{D}_h^{per}$ we let

$$r_n = \rho^d\left(\omega_\phi, s_n\right) / \sup_{y\in\mathbb{R}} \rho^d(y, s_n) = \rho^d\left(\omega_\phi, s_n\right)$$

and define $\Gamma_{h,\Omega,T}$ as

$$\Gamma_{h,\Omega,T} = \left\{ (y_j, s_n) \text{ for } j, n \in \mathbb{Z} \,|\, \phi_h(y_j, s_n) > r_n \sup_{y'} \phi_h(y', s_n), (y', s_n) \in \mathcal{D}_h^{per} \right\}.$$

The fact that the method described above approximates the domain $\Gamma_{\Omega,T}$ reasonably well in practice is illustrated by our numerical experiments.

4.7 Numerical results

4.7.1 The global a posteriori error estimate

In Table 4.2 we show the results for the computational effectivity indexes for smooth solutions of problems (L1), (C), and (NC). We show the L^∞-norm of the difference between the viscosity solution u and the approximation v, the order of convergence of the scheme, the a posteriori error estimate, and the computational effectivity index. The graphs of the computational effectivity indexes as functions of $|\log(\Delta x)|$ are given in Figure 4.2(a),(c),(e). We see that in each of the three

problems, the monotone scheme converges linearly, as expected, and that the computational effectivity index is independent of the mesh size Δx. In all of these cases, the values of the parameters ϵ_x and ϵ_t that minimize the nonlinear functional of the error estimate are equal to 0, in agreement with our discussion in Chapter 3.

Table 4.3 contains the results when the exact solutions of our test problems are nonsmooth. Figure 4.2(b),(d),(f) displays the computational effectivity indexes as functions of $|\log(\Delta x)|$. We can see that even for a nonsmooth viscosity solution the computational effectivity index for a linear Hamiltonian is nearly optimal. For problems (C) and (NC), the computational effectivity indexes increase faster as we decrease the mesh size Δx. Even in these cases, however, the computational effectivity indexes remain relatively small in magnitude and are proportional to $|\log(\Delta x)|$.

In Table 4.4 we show the optimal values of the auxiliary parameter $\epsilon = (\epsilon_x, \epsilon_t)$ for problems (L2), (C), and (NC), when the viscosity solutions are nonsmooth. In the third column, we show on how many values of $\epsilon = (\epsilon_x, \epsilon_t)$ the nonlinear functional of the error estimate has to be evaluated before hitting its minimum. The last column shows the ratio of the optimal values of the auxiliary parameters to the largest values that we allow them to have in the set (4.2). A reasonable choice for the auxiliary parameters would result in a relatively stable ratio, as is the case for all test problems.

As we mentioned earlier, the paraboloid test can be used to detect the location of the kinks in the exact solutions. This fact is illustrated in Figure 4.3. We show the paths of the kinks in the viscosity solutions along with the points from the computational domains $\mathcal{D}_h^{per}$ that fail the paraboloid test when the mesh size $\Delta x = 2/1280$. Note that even though the viscosity solution of problem (L2) is

Table 4.2: Computational effectivity index of the global a posteriori error estimate for **smooth** exact solutions.

Problem	$2/\Delta x$ $(T/\Delta t)$	$\| u - v \|_{L^\infty(\Omega^{per}_{h,T})}$	order	$\Phi_h(v)$	$ei_h(u,v)$
(L1)	20 (10)	5.98e–02	–	6.10e–02	**1.02**
	40 (20)	2.73e–02	1.13	2.77e–02	**1.01**
	80 (40)	1.30e–02	1.07	1.31e–02	**1.01**
	160 (80)	6.33e–03	1.04	6.35e–03	**1.00**
	320 (160)	3.12e–03	1.02	3.13e–03	**1.00**
	640 (320)	1.55e–03	1.01	1.55e–03	**1.00**
	1280 (640)	7.73e–04	1.01	7.73e–04	**1.00**
(C)	20 (10)	6.86e–02	–	7.86e–02	**1.15**
	40 (20)	3.90e–02	0.82	4.95e–02	**1.27**
	80 (40)	2.08e–02	0.91	2.95e–02	**1.42**
	160 (80)	1.07e–02	0.95	1.65e–02	**1.54**
	320 (160)	5.49e–03	0.97	8.83e–03	**1.61**
	640 (320)	2.77e–03	0.99	4.59e–03	**1.66**
	1280 (640)	1.39e–03	1.00	2.34e–03	**1.69**
(NC)	20 (10)	4.34e–02	–	4.68e–02	**1.08**
	40 (20)	1.98e–02	1.13	2.36e–02	**1.19**
	80 (40)	9.16e–03	1.11	1.18e–02	**1.29**
	160 (80)	4.34e–03	1.08	5.86e–03	**1.35**
	320 (160)	2.11e–03	1.04	2.90e–03	**1.38**
	640 (320)	1.03e–03	1.03	1.44e–03	**1.39**
	1280 (640)	5.11e–04	1.02	7.19e–04	**1.41**

Table 4.3: Computational effectivity index of the global a posteriori error estimate for **nonsmooth** exact solutions.

Problem	$2/\Delta x$ $(T/\Delta t)$	$\| u - v \|_{L^\infty(\Omega_{h,T}^{per})}$	order	$\Phi_h(v)$	$ei_h(u,v)$
(L2)	20 (10)	6.16e–02	–	9.64e–02	**1.57**
	40 (20)	4.43e–02	0.47	6.31e–02	**1.42**
	80 (40)	3.46e–02	0.36	4.41e–02	**1.27**
	160 (80)	2.33e–02	0.57	2.86e–02	**1.23**
	320 (160)	1.63e–02	0.52	2.05e–02	**1.25**
	640 (320)	1.14e–02	0.51	1.41e–02	**1.24**
	1280 (640)	8.00e–03	0.51	9.98e–03	**1.25**
(C)	20 (10)	1.13e–01	–	1.57e–01	**1.39**
	40 (20)	6.98e–02	0.70	1.23e–01	**1.76**
	80 (40)	4.05e–02	0.78	9.44e–02	**2.33**
	160 (80)	2.19e–02	0.89	6.05e–02	**2.77**
	320 (160)	1.09e–02	1.01	4.26e–02	**3.92**
	640 (320)	5.13e–03	1.08	3.04e–02	**5.92**
	1280 (640)	2.46e–03	1.06	2.13e–02	**8.65**
(NC)	20 (10)	9.71e–02	–	1.48e–01	**1.53**
	40 (20)	4.81e–02	1.01	1.28e–01	**2.66**
	80 (40)	2.96e–02	0.70	1.09e–01	**3.68**
	160 (80)	1.80e–02	0.72	7.74e–02	**4.29**
	320 (160)	9.44e–03	0.93	5.08e–02	**5.37**
	640 (320)	5.04e–03	0.91	3.53e–02	**7.00**
	1280 (640)	2.54e–03	0.99	2.52e–02	**9.82**

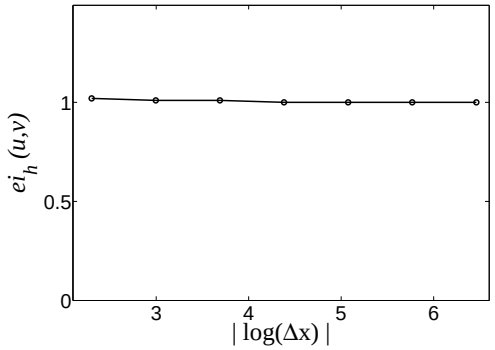

(a) Problem (L1): smooth solution

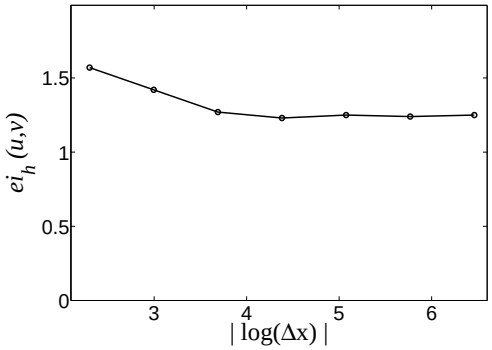

(b) Problem (L2): nonsmooth solution

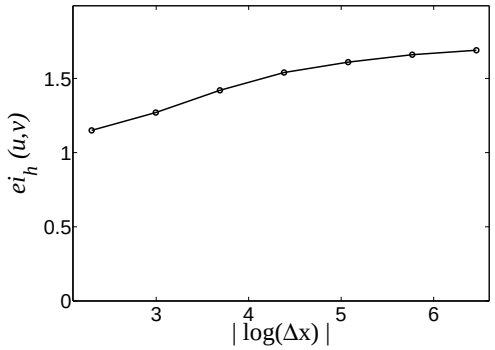

(c) Problem (C): smooth solution

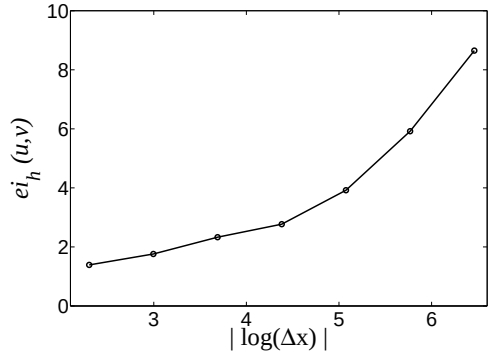

(d) Problem (C): nonsmooth solution

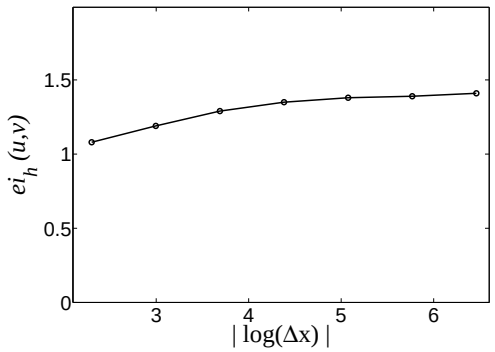

(e) Problem (NC): smooth solution

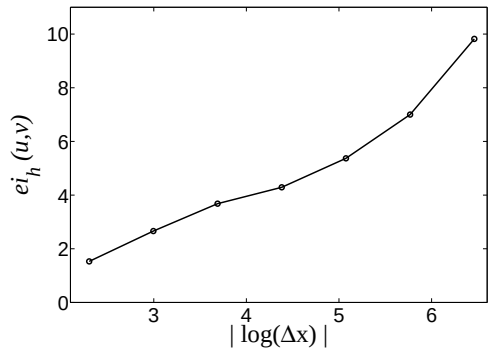

(f) Problem (NC): nonsmooth solution

Figure 4.2: Computational effectivity index as a function of $|\log(\Delta x)|$.

Table 4.4: Parameter $\epsilon = (\epsilon_x, \epsilon_t)$ for **nonsmooth** exact solutions.

Problem	$2/\Delta x$ $(T/\Delta t)$	optimal (ϵ_x, ϵ_t)	ϵ-steps	ratio
(L2)	20 (10)	(0.00e+00, 0.00e+00)	0	0.00
	40 (20)	(4.69e–02, 7.03e–03)	5	0.31
	80 (40)	(3.28e–02, 4.92e–03)	7	0.37
	160 (80)	(2.11e–02, 3.16e–03)	9	0.41
	320 (160)	(1.52e–02, 2.29e–03)	13	0.52
	640 (320)	(1.05e–02, 1.58e–03)	18	0.67
	1280 (640)	(7.32e–03, 1.10e–03)	25	0.83
(C)	20 (10)	(0.00e+00, 0.00e+00)	0	0.00
	40 (20)	(1.00e–01, 4.00e–02)	4	0.33
	80 (40)	(7.50e–02, 3.00e–02)	6	0.40
	160 (80)	(4.38e–02, 1.75e–02)	7	0.39
	320 (160)	(3.13e–02, 1.25e–02)	10	0.48
	640 (320)	(2.34e–02, 9.38e–03)	15	0.63
	1280 (640)	(1.64e–02, 6.56e–03)	21	0.81
(NC)	20 (10)	(0.00e+00, 0.00e+00)	0	0.00
	40 (20)	(0.00e+00, 0.00e+00)	0	0.00
	80 (40)	(1.88e–02, 2.85e–03)	3	0.17
	160 (80)	(1.56e–02, 2.37e–03)	5	0.24
	320 (160)	(9.38e–03, 1.42e–03)	6	0.25
	640 (320)	(7.03e–03, 1.07e–03)	9	0.35
	1280 (640)	(5.08e–03, 7.72e–04)	13	0.45

nonsmooth for all $t \in [0, T]$, we can capture the location of the kink for a certain period only. The reason is that the artificial diffusion term in the monotone scheme causes the approximate solution to 'smooth out' as time increases, and after a certain point in time no points fail the paraboloid test near the kink in the viscosity solution. This can be overcome by considering a finer mesh.

At time $T = 0$, the kink in the viscosity solution of problem (L2) is at $x = 0$. For test problem (C), the location of the kink in the viscosity solution at time $T = 0.40$ is at $x = -0.60$, and for test problem (NC), the kinks in the viscosity solution at time $T = 1.5/\pi^2$ are at $x_1 = -0.8930$ and $x_2 = 0.2438$. Table 4.5 shows the interval $[a, b]$ at the first time level in the computational domain for problem (L2) and the last time level for problems (C) and (NC) over which the paraboloid test fails, i.e., the interval containing the set of points for which condition (3.8) is not satisfied. We can see that as we refine the mesh, more points fail the paraboloid test, and the interval $[a, b]$ gets smaller. Note that for problem (C) we are able to capture the location of the kink even for a relatively coarse mesh. The kinks in the exact solution of problem (NC) are not as 'pointed' as the kink in problem (C) (see Figure 4.1(d),(f)). Because of this fact, we are not able to capture the location of the kinks when we use very coarse meshes.

4.7.2 The local a posteriori error estimate

In this section we study the efficiency of the local a posteriori error estimate with $Q_{h,T}$ and $\Gamma_{h,\Omega,T}$ as the computational domains when applied to problems (L2), (C), and (NC).

Test problem (L2). For problem (L2) we consider the intervals $[-0.15, 0.00]$, $[0.00, 0.15]$, and $[0.30, 0.45]$ at time $T = 0.15$. The viscosity solution has a kink

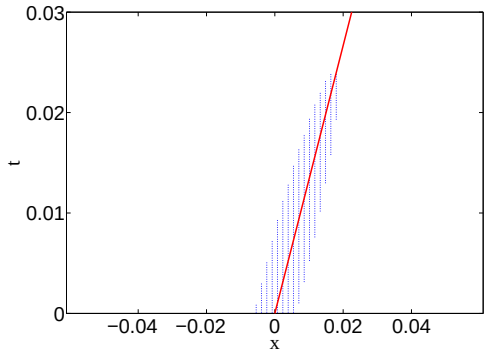

(a) Problem (L2)

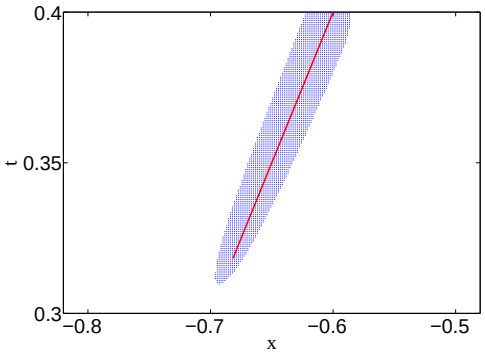

(b) Problem (C)

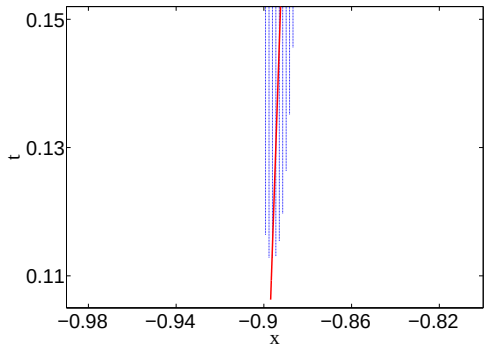

(c) Problem (NC); kink 1

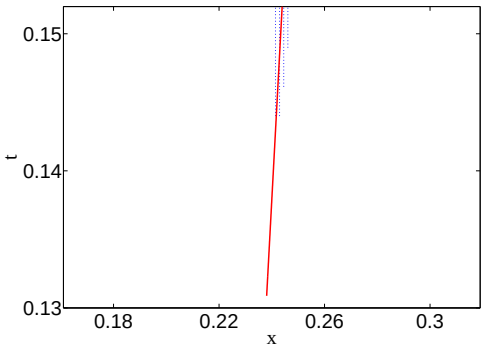

(d) Problem (NC); kink 2

Figure 4.3: Grid points that fail the paraboloid test around the kinks when $2/\Delta x = 1280$.

Table 4.5: **Paraboloid test**: the interval $[a, b]$ for which the paraboloid test fails at the first time level of the computational domain for problem (L2) and the last time level for problems (C) and (NC); the number of grid points inside the interval $[a, b]$.

Problem	$2/\Delta x$	a	b	number of points inside $[a, b]$
(L2)	40	-0.0500	0.0500	2
	80	-0.0250	0.0250	2
	160	-0.0125	0.0250	3
	320	-0.0125	0.0125	4
	640	-0.0094	0.0094	6
	1280	-0.0063	0.0063	8
(C)	40	-0.7500	-0.6000	3
	80	-0.7000	-0.5750	5
	160	-0.6625	-0.5750	7
	320	-0.6438	-0.5750	11
	640	-0.6344	-0.5813	17
	1280	-0.6219	-0.5859	23
(NC) kink 1	80	-0.9250	-0.8750	2
	160	-0.9125	-0.8750	3
	320	-0.9063	-0.8813	4
	640	-0.9031	-0.8844	6
	1280	-0.9000	-0.8859	9
(NC) kink 2	640	0.2406	0.2469	2
	1280	0.2406	0.2469	4

inside the interval $[0.00, 0.15]$. It is smooth inside the interval $[-0.15, 0.00]$, but the region enclosed by its corresponding trapezoid Q_T contains a part of the path of the kink. The viscosity solution is smooth inside the interval $[0.30, 0.45]$, as well as inside its corresponding trapezoid Q_T.

We show the regions enclosed by the trapezoids Q_T corresponding to these intervals together with the characteristics that hit the intervals exactly at their endpoints and the sets of points from $\Gamma_{h,\Omega,T}$ when $\Delta x = 2/160$ in Figure 4.4(a),(c),(e). We see that the method described earlier gives a set of points $\Gamma_{h,\Omega,T}$ that almost perfectly matches the set of points from $\mathcal{D}_h^{per}$ that lie inside $\Gamma_{\Omega,T}$.

In Table 4.6 we show the L^∞-norm of the difference between the viscosity solution u and the approximation v in each interval, the order of convergence of the scheme, the a posteriori error estimate, and the computational effectivity index when $Q_{h,T}$ and $\Gamma_{h,\Omega,T}$ are used as the computational domains. Figure 4.4(b),(d),(f) shows the computational effectivity indexes as functions of $|\log(\Delta x)|$.

As expected, for both computational domains the smallest effectivity indexes are obtained for the interval $[0.30, 0.45]$; the viscosity solution is smooth both inside the interval at time T and inside the trapezoid Q_T. When Q_T is used, the error estimate has the largest computational effectivity index for the interval $[-0.15, 0.00]$, where the viscosity solution is smooth, but whose corresponding Q_T contains a part of the path of the kink. Replacing $Q_{h,T}$ by $\Gamma_{h,\Omega,T}$ significantly improves the efficiency of the error estimate in this case. For both computational domains, the computational effectivity index remains relatively small and close to 1 for the interval $[0.00, 0.15]$, where the viscosity solutions has a discontinuous derivative.

Table 4.7 contains information about the optimal values of the auxiliary parameters ϵ_x and ϵ_t for both computational domains $Q_{h,T}$ and $\Gamma_{h,\Omega,T}$. The ratio

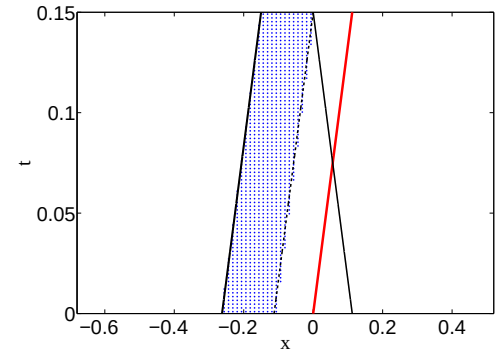

(a) $\Omega = [-0.15, 0.00]$

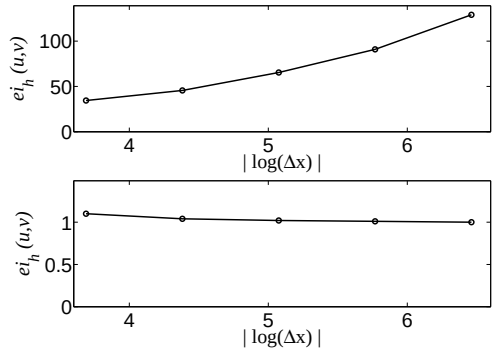

(b) top: $Q_{h,T}$; bottom: $\Gamma_{h,\Omega,T}$

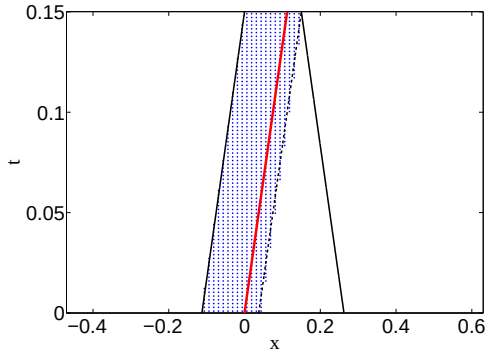

(c) $\Omega = [0.00, 0.15]$

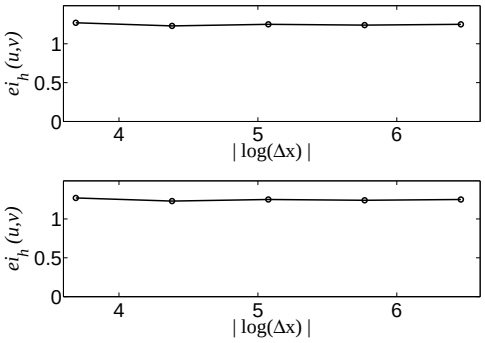

(d) top: $Q_{h,T}$; bottom: $\Gamma_{h,\Omega,T}$

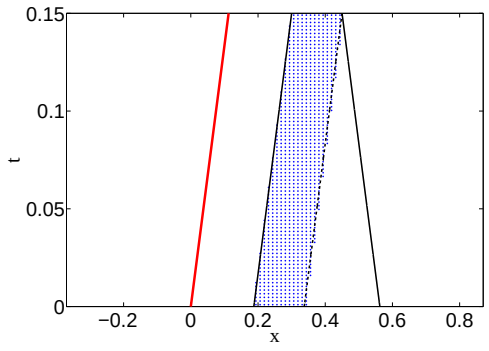

(e) $\Omega = [0.30, 0.45]$

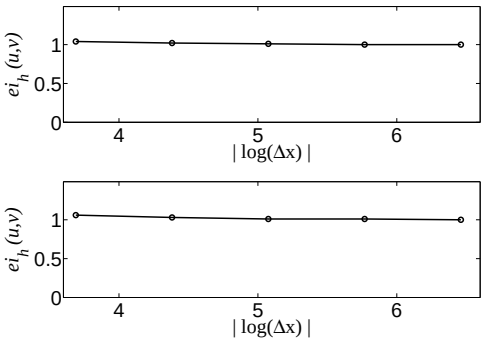

(f) top: $Q_{h,T}$; bottom: $\Gamma_{h,\Omega,T}$

Figure 4.4: **Problem (L2)**; (a),(c),(e): trapezoid Q_T (legs are given by the solid black lines); characteristics that hit the interval Ω exactly at the endpoints (dashed lines; left one coincides with the left leg of Q_T); path of the kink (red line); points from $\Gamma_{h,\Omega,T}$ when $\Delta x = 2/160$); (b),(d),(f): computational effectivity index as a function of $|\log(\Delta x)|$.

Table 4.6: Computational effectivity indexes for problem (L2).

Interval	$\frac{2}{\Delta x}\left(\frac{T}{\Delta t}\right)$	$\| u - v \|_{L^\infty(\Omega_{h,T})}$	order	$Q_{h,T}$		$\Gamma_{h,\Omega,T}$	
				$\Phi_h(v)$	$ei_h(u,v)$	$\Phi_h(v)$	$ei_h(u,v)$
$[-0.15, 0.00]$	80 (40)	1.29e–03	–	4.41e–02	**34.45**	1.40e–03	**1.10**
	160 (80)	6.29e–04	1.02	2.86e–02	**45.57**	6.54e–04	**1.04**
	320 (160)	3.11e–04	1.01	2.04e–02	**65.36**	3.17e–04	**1.02**
	640 (320)	1.55e–04	1.01	1.41e–02	**90.93**	1.56e–04	**1.01**
	1280 (640)	7.73e–05	1.00	9.98e–03	**129.03**	7.77e–05	**1.00**
$[0.00, 0.15]$	80 (40)	3.46e–02	–	4.41e–02	**1.27**	4.41e–02	**1.27**
	160 (80)	2.33e–02	0.57	2.86e–02	**1.23**	2.86e–02	**1.23**
	320 (160)	1.63e–02	0.52	2.04e–02	**1.25**	2.04e–02	**1.25**
	640 (320)	1.14e–02	0.51	1.41e–02	**1.24**	1.41e–02	**1.24**
	1280 (640)	8.00e–03	0.51	9.98e–03	**1.25**	9.98e–03	**1.25**
$[0.30, 0.45]$	80 (40)	5.34e–03	–	5.56e–03	**1.04**	5.65e–03	**1.06**
	160 (80)	2.61e–03	1.03	2.66e–03	**1.02**	2.68e–03	**1.03**
	320 (160)	1.29e–03	1.01	1.31e–03	**1.01**	1.31e–03	**1.01**
	640 (320)	6.44e–04	1.01	6.47e–04	**1.00**	6.48e–04	**1.01**
	1280 (640)	3.21e–04	1.00	3.22e–04	**1.00**	3.22e–04	**1.00**

of the optimal auxiliary parameters to the maximum values allowed by set (4.2) remains stable as the mesh size decreases by a few orders of magnitude, confirming that we have suitably chosen the set for the parameters. As expected, the optimal values of the auxiliary parameters ϵ_x and ϵ_t are 0 when the exact solution is smooth inside the interval Ω and the domains Q_T and $\Gamma_{\Omega,T}$.

Test problem (C). For problem (C) we consider the intervals $[-0.90, -0.75]$, $[-0.70, -0.55]$, and $[0.00, 0.15]$ at $T = 0.40$. The viscosity solution has a discontinuous derivative in the interval $[-0.70, -0.55]$. In $[-0.90, -0.75]$, the viscosity solution is smooth; however, the region enclosed by its corresponding Q_T contains a part of the path of the kink in the viscosity solution. The solution is smooth inside the interval $[0.00, 0.15]$, as well as inside the trapezoid Q_T.

We show the regions enclosed by the trapezoids Q_T corresponding to these intervals and the sets of points from $\Gamma_{h,\Omega,T}$ when $\Delta x = 2/160$ in Figure 4.5(a),(c),(e). Again note that the set of points $\Gamma_{h,\Omega,T}$ matches the set of points from $\mathcal{D}_h^{per}$ that lie inside $\Gamma_{\Omega,T}$ almost perfectly for the intervals $[-0.90, -0.75]$ and $[-0.70, -0.55]$ and reasonably well for the interval $[0.00, 0.15]$. We show the results for the computational effectivity indexes in Table 4.8 and Figure 4.5(b),(d),(f) displays the computational effectivity indexes as functions of $|\log(\Delta x)|$.

The lowest computational effectivity indexes are obtained for the interval $[0.00, 0.15]$ for both domains, as expected. When $Q_{h,T}$ is used as the computational domain, the error estimate has the largest computational effectivity index for the interval $[-0.90, -0.75]$, where the viscosity solution is smooth, but whose corresponding Q_T contains a part of the path of the kink. The improvement in the computational effectivity index for this interval when we replace $Q_{h,T}$ by $\Gamma_{h,\Omega,T}$ as the computational domain is significant. The results for the interval

Table 4.7: Parameter $\epsilon = (\epsilon_x, \epsilon_t)$ for problem (L2).

Interval	Computational domain	$2/\Delta x$ $(T/\Delta t)$	optimal (ϵ_x, ϵ_t)	ϵ-steps	ratio
$[-0.15, 0.00]$	$Q_{h,T}$	80 (40)	(3.28e–02, 4.92e–03)	7	0.37
		160 (80)	(2.11e–02, 3.16e–03)	9	0.41
		320 (160)	(1.52e–02, 2.29e–03)	13	0.52
		640 (320)	(1.05e–02, 1.58e–03)	18	0.67
		1280 (640)	(7.32e–03, 1.10e–03)	25	0.83
$[0.00, 0.15]$	$Q_{h,T}$	80 (40)	(3.28e–02, 4.92e–03)	7	0.37
		160 (80)	(2.11e–02, 3.16e–03)	9	0.41
		320 (160)	(1.52e–02, 2.29e–03)	13	0.52
		640 (320)	(1.05e–02, 1.58e–03)	18	0.67
		1280 (640)	(7.32e–03, 1.10e–03)	25	0.83
$[0.00, 0.15]$	$\Gamma_{h,\Omega,T}$	80 (40)	(3.28e–02, 4.92e–03)	7	0.37
		160 (80)	(2.11e–02, 3.16e–03)	9	0.41
		320 (160)	(1.52e–02, 2.29e–03)	13	0.52
		640 (320)	(1.05e–02, 1.58e–03)	18	0.67
		1280 (640)	(7.32e–03, 1.10e–03)	25	0.83

$[-0.70, -0.55]$ that contains the kink in the viscosity solution are similar for both computational domains. The computational effectivity index for this interval is larger compared to the computational effectivity indexes for the intervals where the viscosity solution is smooth; however, it is still proportional to $|\log(\Delta x)|$. Table 4.9 shows the optimal values of the auxiliary parameters ϵ_x and ϵ_t.

Test problem (NC). For problem (NC) we consider five different intervals for which we compute the computational effectivity index when $T = 1.5/\pi^2$. The viscosity solution has a discontinuous derivative in the intervals $[-0.95, -0.80]$ and $[0.15, 0.30]$. In the intervals $[-0.88, -0.73]$ and $[0.08, 0.23]$, the viscosity solution is smooth; however, the regions enclosed by their corresponding trapezoids Q_T contain parts of the paths of the two kinks. Finally, the viscosity solution is smooth inside the interval $[-0.30, -0.15]$, as well as inside its corresponding Q_T. We show the regions enclosed by the trapezoid Q_T and the sets of points from $\Gamma_{h,\Omega,T}$ for these intervals in Figure 4.6(a),(c),(e) and Figure 4.7 (a),(c).

Table 4.10 contains the results for the computational effectivity indexes and Figures 4.6(b),(d),(f) and 4.7(b),(d) show the computational effectivity indexes as functions of $|\log(\Delta x)|$. The results are similar to the results for test problem (C). As expected, the smallest effectivity index is obtained in the cases when the viscosity solution is smooth in the interval of consideration and inside its corresponding domains Q_T and $\Gamma_{\Omega,T}$. The computational effectivity indexes for the intervals $[-0.95, -0.80]$ and $[0.15, 0.30]$ that contain the kinks in the viscosity solution are proportional to $|\log(\Delta x)|$ and remain reasonably small as we refine the mesh for both computational domains. The largest effectivity indexes are again obtained for the intervals where the viscosity solution is smooth, but whose corresponding trapezoids Q_T contain parts of the paths of the kinks in viscosity

Table 4.8: Computational effectivity indexes for problem (C).

Interval	$\frac{2}{\Delta x}\left(\frac{T}{\Delta t}\right)$	$\| u - v \|_{L^\infty(\Omega_{h,T})}$	order	$Q_{h,T}$		$\Gamma_{h,\Omega,T}$	
				$\Phi_h(v)$	$ei_h(u,v)$	$\Phi_h(v)$	$ei_h(u,v)$
$[-0.90, -0.75]$	80 (40)	3.30e–03	–	8.55e–02	**25.90**	4.89e–03	**1.48**
	160 (80)	1.66e–03	0.99	6.05e–02	**36.53**	2.23e–03	**1.35**
	320 (160)	8.29e–04	1.00	4.26e–02	**51.40**	1.07e–03	**1.29**
	640 (320)	4.14e–04	1.00	3.04e–02	**73.30**	5.22e–04	**1.26**
	1280 (640)	2.06e–04	1.01	2.13e–02	**103.16**	2.63e–04	**1.27**
$[-0.70, -0.55]$	80 (40)	4.05e–02	–	9.02e–02	**2.22**	8.66e–02	**2.14**
	160 (80)	2.19e–02	0.89	6.05e–02	**2.77**	6.05e–02	**2.77**
	320 (160)	1.09e–02	1.01	4.26e–02	**3.92**	4.26e–02	**3.92**
	640 (320)	5.13e–03	1.08	3.01e–02	**5.87**	3.01e–02	**5.86**
	1280 (640)	2.46e–03	1.06	2.12e–02	**8.62**	2.12e–02	**8.61**
$[0.00, 0.15]$	80 (40)	1.76e–02	–	2.69e–02	**1.53**	2.69e–02	**1.53**
	160 (80)	8.85e–03	0.99	1.35e–02	**1.53**	1.35e–02	**1.53**
	320 (160)	4.43e–03	1.00	6.76e–03	**1.52**	6.75e–03	**1.52**
	640 (320)	2.21e–03	1.00	3.38e–03	**1.53**	3.38e–03	**1.52**
	1280 (640)	1.10e–03	1.00	1.69e–03	**1.53**	1.69e–03	**1.53**

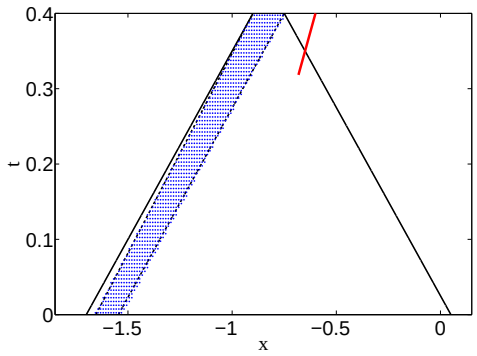

(a) $\Omega = [-0.90, -0.75]$

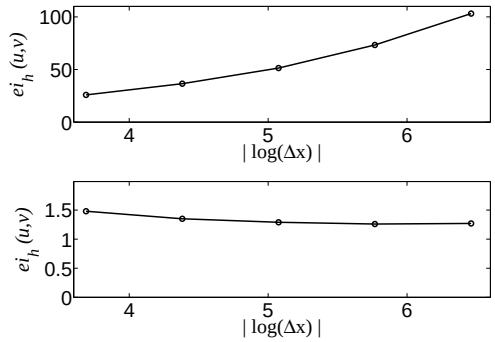

(b) top: $Q_{h,T}$; bottom: $\Gamma_{h,\Omega,T}$

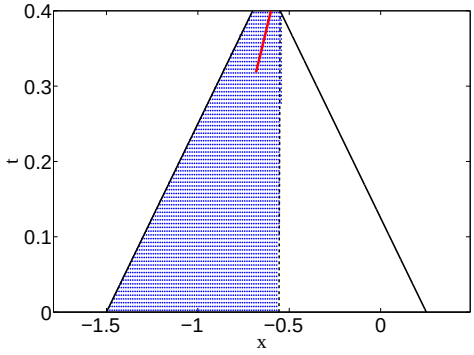

(c) $\Omega = [-0.70, -0.55]$

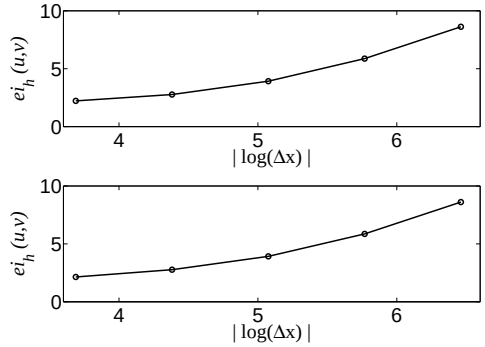

(d) top: $Q_{h,T}$; bottom: $\Gamma_{h,\Omega,T}$

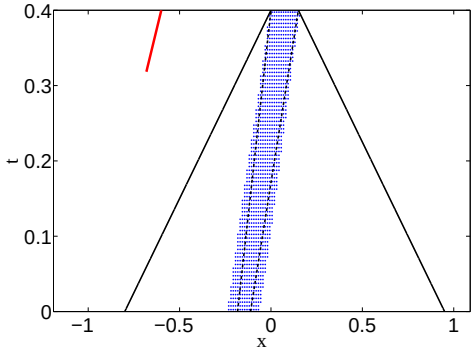

(e) $\Omega = [0.00, 0.15]$

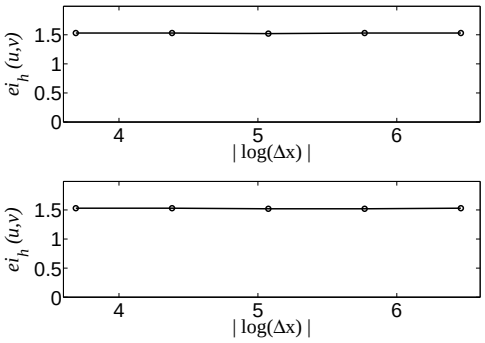

(f) top: $Q_{h,T}$; bottom: $\Gamma_{h,\Omega,T}$

Figure 4.5: **Problem (C)**; (a),(c),(e): trapezoid Q_T (legs are given by the solid black lines); characteristics that hit the interval Ω exactly at the endpoints (dashed lines); path of the kink (red line); points from $\Gamma_{h,\Omega,T}$ when $\Delta x = 2/160$); (b),(d),(f): computational effectivity index as a function of $|\log(\Delta x)|$.

Table 4.9: Parameter $\epsilon = (\epsilon_x, \epsilon_t)$ for problem (C).

Interval	Computational domain	$2/\Delta x$ $(T/\Delta t)$	optimal (ϵ_x, ϵ_t)	ϵ-steps	ratio
$[-0.90, -0.75]$	$Q_{h,T}$	80 (40)	(6.25e–02, 2.50e–02)	5	0.33
		160 (80)	(4.38e–02, 1.75e–02)	7	0.39
		320 (160)	(3.13e–02, 1.25e–02)	10	0.48
		640 (320)	(2.34e–02, 9.38e–03)	15	0.63
		1280 (640)	(1.64e–02, 6.56e–03)	21	0.81
$[-0.70, -0.55]$	$Q_{h,T}$	80 (40)	(7.50e–02, 3.00e–02)	6	0.40
		160 (80)	(4.38e–02, 1.75e–02)	7	0.39
		320 (160)	(3.13e–02, 1.25e–02)	10	0.48
		640 (320)	(2.34e–02, 9.38e–03)	15	0.63
		1280 (640)	(1.64e–02, 6.56e–03)	21	0.81
$[-0.70, -0.55]$	$\Gamma_{h,\Omega,T}$	80 (40)	(7.50e–02, 3.00e–02)	6	0.40
		160 (80)	(4.38e–02, 1.75e–02)	7	0.39
		320 (160)	(3.13e–02, 1.25e–02)	10	0.48
		640 (320)	(2.34e–02, 9.38e–03)	15	0.63
		1280 (640)	(1.64e–02, 6.56e–03)	21	0.81

solution, i.e., the intervals $[-0.88, -0.73]$ and $[0.08, 0.23]$. Replacing $Q_{h,T}$ by $\Gamma_{h,\Omega,T}$ for these intervals results in significantly lower computational indexes that remain close to 1 throughout the large variation of the sizes of Δx and Δt.

Table 4.11 contains the information about the optimal values of the auxiliary parameter $\epsilon = (\epsilon_x, \epsilon_t)$. The optimal values for ϵ_x and ϵ_t in the cases when the viscosity solution is smooth inside the intervals and inside the domains Q_T and $\Gamma_{\Omega,T}$ are 0, as expected. Note that, even though the region enclosed by the trapezoid Q_T corresponding to the interval $[0.08, 0.23]$ contains a part of the path of the kink in the viscosity solution, the values of the auxiliary parameters are equal to 0. The reason is that the kink inside Q_T is relatively 'mild' (see Figure 4.1(f)). For the cases involving a kink in the exact solution, the ratio of the optimal auxiliary parameters to the maximum values that are allowed in the set (4.2) remains relatively stable as the mesh gets refined, indicating that this choice for the set of values for the parameters ϵ_x and ϵ_t is reasonable.

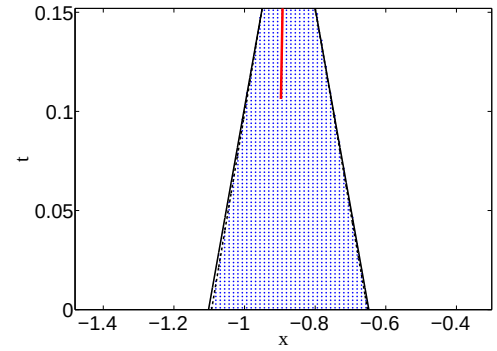

(a) $\Omega = [-0.95, -0.80]$

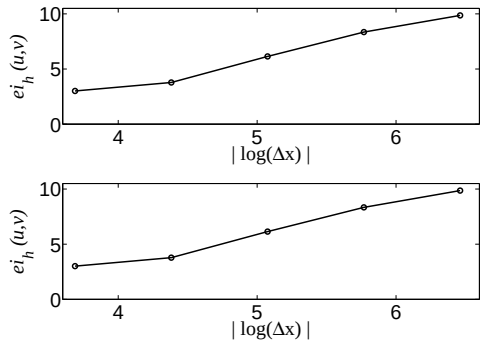

(b) top: $Q_{h,T}$; bottom: $\Gamma_{h,\Omega,T}$

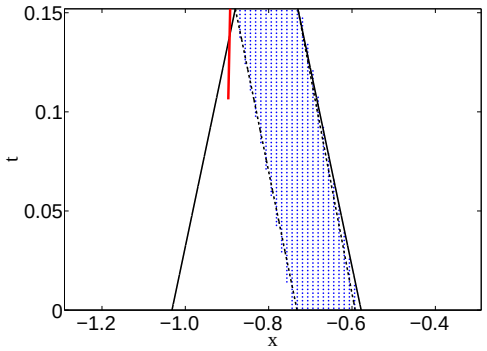

(c) $\Omega = [-0.88, -0.73]$

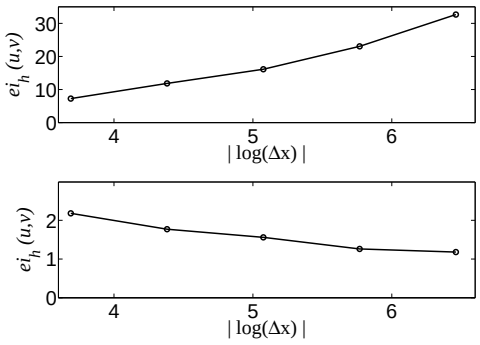

(d) top: $Q_{h,T}$; bottom: $\Gamma_{h,\Omega,T}$

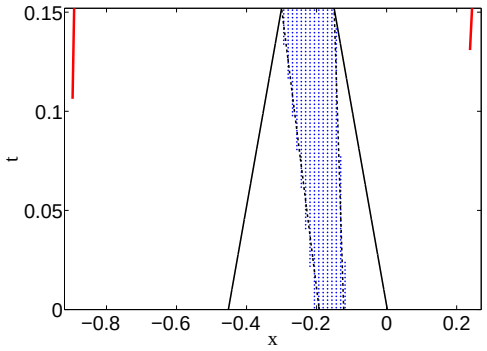

(e) $\Omega = [-0.30, -0.15]$

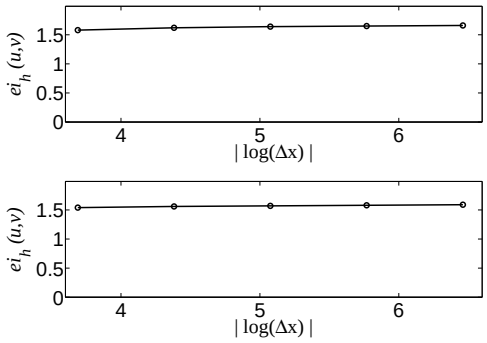

(f) top: $Q_{h,T}$; bottom: $\Gamma_{h,\Omega,T}$

Figure 4.6: **Problem (NC), part 1**; (a),(c),(e): trapezoid Q_T (legs are given by the solid black lines); characteristics that hit the interval Ω exactly at the endpoints (dashed lines); path of the kink (red line); points from $\Gamma_{h,\Omega,T}$ when $\Delta x = 2/160$); (b),(d),(f): computational effectivity index as a function of $|\log(\Delta x)|$.

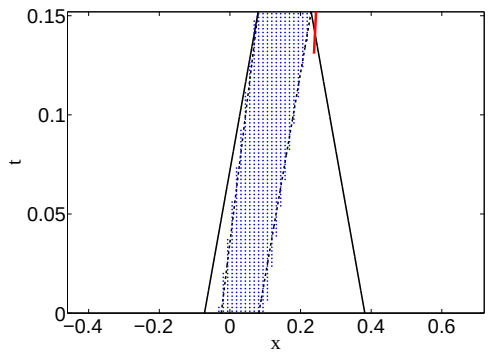

(a) $\Omega = [0.08, 0.23]$

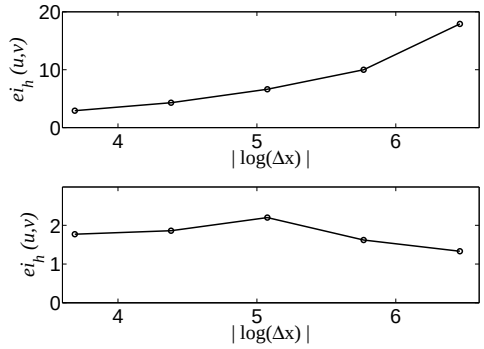

(b) top: $Q_{h,T}$; bottom: $\Gamma_{h,\Omega,T}$

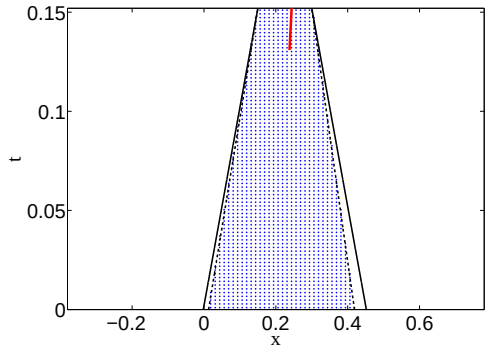

(c) $\Omega = [0.15, 0.30]$

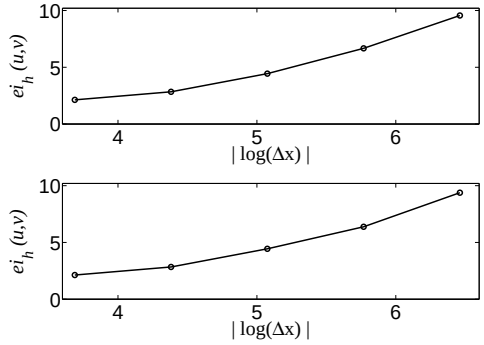

(d) top: $Q_{h,T}$; bottom: $\Gamma_{h,\Omega,T}$

Figure 4.7: **Problem (NC), part 2**; (a),(c): trapezoid Q_T (legs are given by the solid black lines); characteristics that hit the interval Ω exactly at the endpoints (dashed lines); path of the kink (red line); points from $\Gamma_{h,\Omega,T}$ when $\Delta x = 2/160$); (b),(d): computational effectivity index as a function of $|\log(\Delta x)|$.

Table 4.10: Computational effectivity indexes for problem (NC).

Interval	$\frac{2}{\Delta x}\left(\frac{T}{\Delta t}\right)$	$\| u - v \|_{L^\infty(\Omega_{h,T})}$	order	$Q_{h,T}$		$\Gamma_{h,\Omega,T}$	
				$\Phi_h(v)$	$ei_h(u,v)$	$\Phi_h(v)$	$ei_h(u,v)$
$[-0.95,-0.80]$	80 (40)	2.96e–02	–	8.90e–02	**3.01**	8.90e–02	**3.01**
	160 (80)	1.80e–02	0.72	6.81e–02	**3.78**	6.81e–02	**3.78**
	320 (160)	7.29e–03	1.31	4.48e–02	**6.14**	4.48e–02	**6.14**
	640 (320)	3.66e–03	0.99	3.06e–02	**8.35**	3.05e–02	**8.34**
	1280 (640)	2.28e–03	0.68	2.25e–02	**9.86**	2.25e–02	**9.86**
$[-0.88,-0.73]$	80 (40)	1.50e–02	–	1.09e–01	**7.25**	3.28e–02	**2.18**
	160 (80)	6.21e–03	1.28	7.36e–02	**11.84**	1.10e–02	**1.77**
	320 (160)	3.10e–03	1.00	4.99e–02	**16.12**	4.84e–03	**1.56**
	640 (320)	1.53e–03	1.02	3.53e–02	**23.05**	1.92e–03	**1.26**
	1280 (640)	7.52e–04	1.03	2.46e–02	**32.66**	8.90e–04	**1.18**
$[-0.30,-0.15]$	80 (40)	1.12e–02	–	1.77e–02	**1.58**	1.73e–02	**1.54**
	160 (80)	5.52e–03	1.02	8.93e–03	**1.62**	8.64e–03	**1.56**
	320 (160)	2.74e–03	1.01	4.49e–03	**1.64**	4.31e–03	**1.57**
	640 (320)	1.36e–03	1.01	2.25e–03	**1.65**	2.15e–03	**1.58**
	1280 (640)	6.77e–04	1.01	1.13e–03	**1.66**	1.08e–03	**1.59**
$[0.08,0.23]$	80 (40)	2.03e–02	–	5.95e–02	**2.92**	3.61e–02	**1.77**
	160 (80)	9.74e–03	1.06	4.22e–02	**4.34**	1.81e–02	**1.86**
	320 (160)	4.98e–03	0.97	3.30e–02	**6.62**	1.10e–02	**2.20**
	640 (320)	2.43e–03	1.04	2.42e–02	**9.99**	3.93e–03	**1.62**
	1280 (640)	1.18e–03	1.04	2.11e–02	**17.91**	1.57e–03	**1.33**
$[0.15,0.30]$	80 (40)	2.85e–02	–	6.07e–02	**2.13**	6.07e–02	**2.13**
	160 (80)	1.80e–02	0.66	5.12e–02	**2.84**	5.12e–02	**2.84**
	320 (160)	9.44e–03	0.93	4.19e–02	**4.44**	4.19e–02	**4.44**
	640 (320)	5.04e–03	0.92	3.37e–02	**6.67**	3.22e–02	**6.38**
	1280 (640)	2.54e–03	0.99	2.43e–02	**9.56**	2.39e–02	**9.38**

Table 4.11: Parameter $\epsilon = (\epsilon_x, \epsilon_t)$ for problem (NC).

Interval	Computational domain	$2/\Delta x$ $(T/\Delta t)$	optimal (ϵ_x, ϵ_t)	ϵ-steps	ratio
$[-0.95, -0.80]$	$Q_{h,T}$	80 (40)	(2.50e–02, 3.80e–03)	4	0.22
		160 (80)	(1.56e–02, 2.37e–03)	5	0.24
		320 (160)	(1.09e–02, 1.66e–03)	7	0.29
		640 (320)	(7.81e–03, 1.19e–03)	10	0.38
		1280 (640)	(5.47e–03, 8.31e–04)	14	0.48
$[-0.88, -0.73]$	$Q_{h,T}$	80 (40)	(0.00e+00, 0.00e+00)	0	0.00
		160 (80)	(1.56e–02, 2.37e–03)	5	0.24
		320 (160)	(1.09e–02, 1.66e–03)	7	0.29
		640 (320)	(7.03e–03, 1.07e–03)	9	0.35
		1280 (640)	(5.08e–03, 7.72e–04)	13	0.45
$[0.15, 0.30]$	$Q_{h,T}$	80 (40)	(0.00e+00, 0.00e+00)	0	0.00
		160 (80)	(0.00e+00, 0.00e+00)	0	0.00
		320 (160)	(0.00e+00, 0.00e+00)	0	0.00
		640 (320)	(7.03e–03, 1.07e–03)	9	0.35
		1280 (640)	(5.08e–03, 7.72e–04)	13	0.45
$[-0.95, -0.80]$	$\Gamma_{h,\Omega,T}$	80 (40)	(2.50e–02, 3.80e–03)	4	0.22
		160 (80)	(1.56e–02, 2.37e–03)	5	0.24
		320 (160)	(1.09e–02, 1.66e–03)	7	0.29
		640 (320)	(7.81e–03, 1.19e–03)	10	0.38
		1280 (640)	(5.47e–03, 8.31e–04)	14	0.48
$[0.15, 0.30]$	$\Gamma_{h,\Omega,T}$	80 (40)	(0.00e+00, 0.00e+00)	0	0.00
		160 (80)	(0.00e+00, 0.00e+00)	0	0.00
		320 (160)	(0.00e+00, 0.00e+00)	0	0.00
		640 (320)	(7.03e–03, 1.07e–03)	9	0.35
		1280 (640)	(5.08e–03, 7.72e–04)	13	0.45

Chapter 5

Conclusion

In this dissertation we obtain a generalization of the global a posteriori error estimate for time-dependent Hamilton-Jacobi equations introduced in [3] that gives an upper bound for the difference between the viscosity solution u of the Cauchy problem (1.1), (1.2) and a continuous function v for any sub-domain of $\mathbb{R}^d$ at time T. We provide numerical experiments studying the efficiency of this local error estimate and the global a posteriori error estimate obtained in [3]. The numerical experiments show that even in the difficult cases of nonlinear Hamiltonians, when the viscosity solution displays kinks, the error estimates applied to a monotone scheme produce effectivity indexes that remain relatively small as the discretization parameters vary in several orders of magnitude.

The results of this dissertation leave open a few problems. First, we have presented a direction that could lead to better approximating the domain that contains the characteristics entering the sub-domain of $\mathbb{R}^d$ in which we compute the approximation error. A rigorous treatment of this topic is highly nontrivial and constitutes the subject of ongoing work. In our numerical experiments we have focused on monotone schemes because they are guaranteed to converge to

the viscosity solution. Monotone schemes are only first order accurate, however. Therefore, the study could be extended to include higher order schemes such as the discontinuous Galerkin scheme developed in [18]. The a posteriori error estimates could be effectively used in adaptive algorithms with rigorous error control for time-dependent Hamilton-Jacobi equations, similar to the algorithms proposed in [7], [9], and [10] for steady-state Hamilton-Jacobi equations. In this case, however, the time-space grids must be allowed to vary locally. The modification of the monotone scheme we have considered that properly handles locally varying time-space grids developed in [24] could be successfully utilized.

Bibliography

[1] R. Abgrall, *Numerical discretization of the first-order Hamilton-Jacobi equation on triangular meshes*, Comm. Pure Appl. Math., **49** (1996), 1339–1373.

[2] S. Albert, B. Cockburn, D. French, and T. Peterson, *A posteriori error estimates for general numerical methods for Hamilton-Jacobi equations. Part I: The steady state case*, Math. Comp. **71** (2002), 49–76.

[3] ———, *A posteriori error estimates for general numerical methods for Hamilton-Jacobi equations. Part II: The time-dependent case*, Finite Volumes for Complex Applications, (R. Herbin and D. Kröner, eds.), vol. III, Hermes Penton Science, June 2002, 17–24.

[4] T. Barth and J. Sethian, *Numerical schemes for Hamilton-Jacobi and level set equations on triangular domains*, J. Comput. Phys. **145** (1998), 1–40.

[5] D. P. Bertsekas, *Dynamic programming and optimal control*, vol. I, Athena Scientific, Belmont, MA, 1995.

[6] A. Bressan, *Viscosity solutions of Hamilton-Jacobi equations and optimal control problems (an illustrated tutorial)*, available at http://www.math.psu.edu/bressan.

[7] Y. Chen and B. Cockburn, *An adaptive high-order discontinuous Galerkin method with error control for time Hamilton-Jacobi equations. Part I: The one-dimensional steady state case*, J. Comput. Phys., **226** (2007), 1027–1058.

[8] B. Cockburn and P. Gremaud, *A priori error estimates for numerical methods for scalar conservation laws. Part I: The general approach*, Math. Comp., **65** (1996), 533–573.

[9] B. Cockburn and B. Yenikaya, *An adaptive method with rigorous error control for the Hamilton-Jacobi equations. Part I: The one-dimensional steady state case*, Appl. Numer. Math., **52** (2005), 175–195.

[10] ———, *An adaptive method with rigorous error control for the Hamilton-Jacobi equations. Part II: The two-dimensional steady state case*, J. Comput. Phys., **209** (2005), 391–405.

[11] M. G. Crandall, L. C. Evans, and P. L. Lions, *Some properties of viscosity solutions of Hamilton-Jacobi equations*, Trans. Amer. Math. Soc. **282** (1984), 478–502.

[12] M. G. Crandall and P. L. Lions, *Viscosity solutions of Hamilton-Jacobi equations*, Trans. Amer. Math. Soc., **277** (1983), 1–42.

[13] ———, *Two approximations of solutions of Hamilton-Jacobi equations*, Math. Comp., **43** (1984), 1–19.

[14] L. C. Evans, *Partial differential equations*, American Mathematical Society, Providence, RI, 1998.

[15] L. C. Evans and P. E. Souganidis, *Differential games and representation formulas for solutions of Hamilton-Jacobi-Isaacs equations*, Indiana Univ. Math. J., **33** (1984), 773–797.

[16] M. Falcone and R. Ferretti, *Discrete time high-order schemes for viscosity solutions of Hamilton-Jacobi-Bellman equations*, Numer. Math., **67** (1994), 315–344.

[17] P. A. Forsyth and G. Labahn, *Numerical methods for controlled Hamilton-Jacobi-Bellman PDEs in finance*, J. Comput. Finance, **11** (2008), 1–44.

[18] C. Hu and C.-W. Shu, *A discontinuous Galerkin finite element method for Hamilton-Jacobi equations*, SIAM J. Sci. Comput., **21** (1999), 666–690.

[19] H. Ishii, *Uniqueness of unbounded viscosity solution of Hamilton-Jacobi equations*, Indiana Univ. Math. Journal **33** (1984), 721–748.

[20] A. Kurganov and G. Petrova, *Adaptive central-upwind schemes for Hamilton-Jacobi equations with nonconvex Hamiltonians*, SIAM J. Sci. Comput., **27** (2006), 323–333.

[21] C.-T. Lin and E. Tadmor, *L^1-stability and error estimates for approximate Hamilton-Jacobi solutions*, Numer. Math. **87** (2001), 701–735.

[22] S. Osher and R. Sanders, *Numerical approximations to nonlinear conservation laws with locally varying time and space grids*, Math. Comp., **41** (1983), 321–336.

[23] S. Osher and C.-W. Shu, *High-order essentially nonoscillatory schemes for Hamilton-Jacobi equations*, SIAM J. Numer. Anal. **28** (1991), 907–922.

[24] J. Qian, *Approximations for viscosity solutions of Hamilton-Jacobi equations with locally varying time and space grids*, SIAM J. Numer. Anal., **43** (2006), 2371–2401.

[25] J. A. Sethian, *Level set methods: evolving interfaces in geometry, fluid mechanics, computer vision, and material science*, Cambridge University Press, Cambridge, 1996.

[26] P. E. Souganidis, *Approximation schemes for viscosity solutions of Hamilton-Jacobi equations*, J. Diff. Eqns., **59** (1985), 1–43.

[27] H.-Z. Tang, T. Tang, and P. Zhang, *An adaptive mesh redistribution method for nonlinear Hamilton-Jacobi equations in two- and three-dimensions*, J. Comput. Phys., **188** (2003), 543–572.

[28] G. B. Whitham, *Linear and nonlinear waves*, Wiley, New York, NY, 1974.